



Universiteit
Leiden
The Netherlands

Computational electrocatalysis: methods and fundamental applications on CO₂ reduction and formic acid oxidation

Granda Marulanda, L.P.

Citation

Granda Marulanda, L. P. (2021, October 19). *Computational electrocatalysis: methods and fundamental applications on CO₂ reduction and formic acid oxidation*. Retrieved from <https://hdl.handle.net/1887/3217519>

Version: Publisher's Version

License: [Licence agreement concerning inclusion of doctoral thesis in the Institutional Repository of the University of Leiden](#)

Downloaded from: <https://hdl.handle.net/1887/3217519>

Note: To cite this publication please use the final published version (if applicable).



Leiden Centraal Station
The Netherlands

A: Supporting Information for Chapter 2

In Figure A1 we show that the PBE-calculated¹ d-band center of the Pt skin on the near-surface alloys studied here linearly correlates with the number of valence electrons of the metals along the 3d, 4d and 5d series. It was previously shown that valence electrons correlate linearly with the d-band centers of various transition metals.^{1,2}

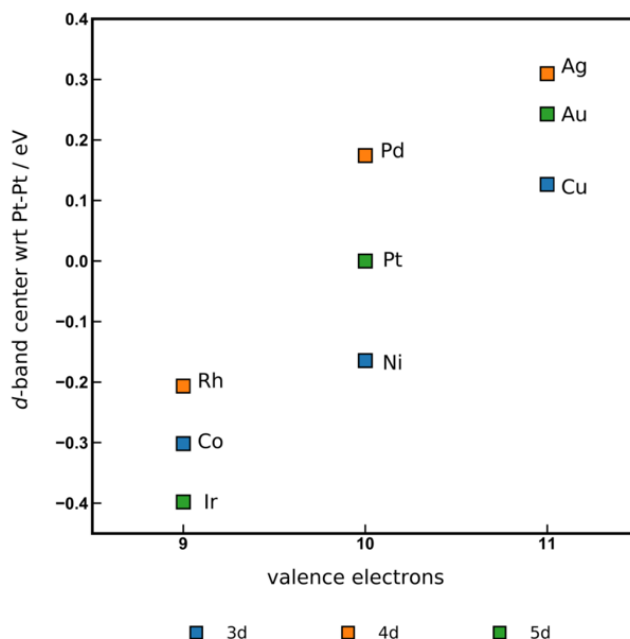
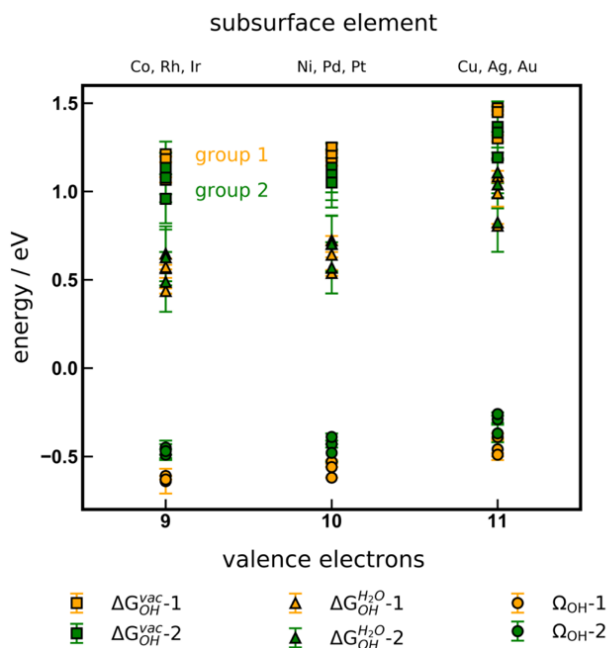
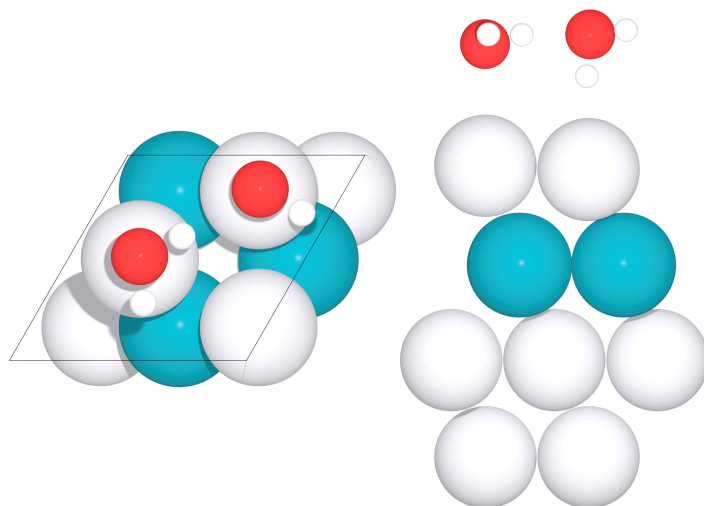


FIGURE A1

D-band center of the Pt skin on the NSAs with respect to the d-band center of the top layer of Pt(111) as a function of the valence electrons of the subsurface metals. A nearly linear correlation between the d-band center and the valence electrons for various metals along the 3d (Co, Ni, Cu), 4d (Rh, Pd, Ag), and 5d (Ir, Pt, Au) series is observed, in line with previous reports.^{1,3}

**FIGURE A2**

Adsorption energies of group 1 functionals (PBE/ PW91) in orange and group 2 functionals (RPBE, vdW and with dispersion corrections) in green as a function of the number of valence electrons of the subsurface metal atom in the Pt NSAs. For both groups, squares represent the energies of 1/3 ML *OH in vacuum (ΔG_{OH}^{vac}) triangles represent the energies of *OH within the water bilayer ($\Delta G_{OH}^{H_2O}$), and circles represent the solvation energy (Ω_{OH}). Solvation energies for group 2 (green) are generally less negative than those of group 1 (orange). The error bars cover the standard deviation of the respective groups of functionals. The correlation between the number of valence electrons and the d-band centers of the Pt skins is provided in Figure A1.

**FIGURE A3**

Top and side view of the water adlayer on a $\sqrt{3}\times\sqrt{3}$ R30° unit cell of Pt (111) NSA. The cell contains 3 metals per atom layer, and 2 water molecules per unit cell. The water molecules are on top of a Pt metal. One water molecule is on the flat configuration and the other one with one hydrogen pointing towards the surface as shown in the side view.

The water adlayer shown in Figure A3 is the ice-like water adlayer structure found to be computationally stable in closed-packed metal surfaces.⁴⁻⁶ This water adlayer of 2/3 ML coverage can be adsorbed with one water molecule in the flat configuration while the other water molecule can be with one hydrogen pointing towards the surface (H-down) or away from it (H-up). The difference in energy between these two configurations is small, about 0.05 eV as reported in the literature based on DFT adsorption energies.^{4,7} Our calculated free energies of adsorption of the water adlayer on Pt(111) show a difference of 0.01 eV between the H-up and H-down configuration being the H-down configuration more stable.

TABLE A1

Free energies of solvation (Ω_{OH}) in eV for 1/3 ML *OH coadsorbed with 1/3 ML *H₂O within a water bilayer using different functionals. Avg1 and avg2 are the averages of the solvation energies for group 1 functionals (PBE, PW91) and group 2 functionals (RPBE, vdW and dispersion corrections) across the same metal. Stdev1/2 are the corresponding standard deviations of avg1/avg2. Avg0 is the average of the solvation energies across the metals for all the functionals and stdev0 is its standard deviation. MAX and MIN are the maximal and minimal values in the dataset across the same functional. Range is the difference between MAX and MIN.^a

metal	PW91	PBE	RPBE	PBE-D3	RPBE-D3	Opt-PBE	BEEF-vdw	avg 0	avg 1	avg 2	stdev 0	stdev 1	stdev 2
Co	-0.60	-0.69	-0.50	-0.45	-	-0.52	-0.48	-0.54	-0.64	-0.49	0.09	0.07	0.03
Rh	-0.61	-0.61	-0.45	-0.47	-0.48	-0.47	-0.39	-0.50	-0.61	-0.45	0.08	0.00	0.04
Ir	-0.63	-0.63	-0.43	-0.50	-0.50	-0.49	-0.43	-0.52	-0.63	-0.47	0.08	0.00	0.04
Ni	-0.53	-0.52	-0.40	-0.43	-0.45	-0.43	-0.44	-0.46	-0.53	-0.43	0.05	0.01	0.02
Pd	-0.56	-0.56	-0.36	-0.40	-0.41	-0.40	-0.39	-0.44	-0.56	-0.39	0.08	0.00	0.02
Pt	-0.62	-0.62	-0.50	-0.45	-0.57	-0.45	-0.44	-0.52	-0.62	-0.48	0.08	0.00	0.05
Cu	-0.50	-0.42	-0.32	-0.31	-0.27	-0.29	-0.28	-0.34	-0.46	-0.29	0.09	0.06	0.02
Ag	-0.40	-0.38	-0.26	-0.25	-0.27	-0.25	-0.27	-0.30	-0.39	-0.26	0.06	0.02	0.01
Au	-0.49	-0.50	-0.35	-0.35	-0.46	-0.35	-0.33	-0.40	-0.49	-0.37	0.08	0.01	0.05
mean	-0.55	-0.55	-0.39	-0.40	-0.43	-0.41	-0.38						
stdev	0.08	0.10	0.08	0.08	0.11	0.09	0.07						
MAX	-0.40	-0.38	-0.26	-0.25	-0.27	-0.25	-0.27						
MIN	-0.63	-0.69	-0.50	-0.50	-0.57	-0.52	-0.48						
range	0.23	0.32	0.24	0.25	0.30	0.27	0.21						
LNDm	-0.08	-0.15	-0.10	-0.10	-0.14	-0.11	-0.10						
LPDm	0.15	0.17	0.14	0.16	0.16	0.16	0.11						
LPDPt	0.22	0.24	0.24	0.21	0.30	0.21	0.17						
LNDPt	-0.01	-0.07	0.00	-0.04	0.00	-0.06	-0.04						
AOM													-0.44
Stdev AOM													0.07
LND_{AOM}													-0.10
LPD_{AOM}													0.06
avg1 across functionals													-0.55
avg2 across functionals													-0.40
Diff avg1 - avg2 across functionals													0.15
Diff avg1 - avg2 across metals													0.14

[a] LNDm/LPDm: Largest negative/positive deviation from the mean

LNDPt/LPDPT: Largest negative/positive deviation from Pt

AOM: Average of the means

Standard deviation of AOM

LND_{AOM}/LPD_{AOM}: Largest negative/positive deviation from the AOM

TABLE A2

Adsorption energies in eV of 1/3 ML *OH in vacuum (ΔG_{OH}^{vac}). avg1 and avg2 are the averages of the solvation energies for group 1 functionals (PBE, PW91) and group 2 functionals (RPBE, vdW and with dispersion corrections) across the same metal. Stdev1/2 are the corresponding standard deviations of avg1/avg2. Avg0 is the average of the solvation energies across the metals for all the functionals and stdev0 is its standard deviation.

metal	PW91	PBE	RPBE	PBE-D3	RPBE-D3	optPBE	BEEF-vdw	avg0	avg1	avg2	stdev0	stdev1	stdev2
Co	1.20	1.22	1.33	1.11	-	0.97	1.12	1.16	1.21	1.13	0.12	0.01	0.15
Rh	1.17	1.19	1.31	1.03	1.02	0.94	1.10	1.11	1.18	1.08	0.13	0.02	0.14
Ir	1.05	1.08	1.19	0.91	0.89	0.82	0.98	0.99	1.07	0.96	0.12	0.02	0.14
Ni	1.23	1.26	1.36	1.08	1.08	0.99	1.15	1.17	1.25	1.13	0.13	0.02	0.14
Pd	1.19	1.21	1.33	1.04	1.04	0.96	1.11	1.12	1.20	1.09	0.13	0.01	0.14
Pt	1.15	1.17	1.28	0.99	0.99	0.91	1.07	1.08	1.16	1.05	0.13	0.01	0.14
Cu	1.44	1.46	1.57	1.28	1.24	1.20	1.37	1.37	1.45	1.33	0.13	0.01	0.15
Ag	1.46	1.48	1.60	1.31	1.29	1.23	1.40	1.40	1.47	1.37	0.13	0.02	0.14
Au	1.29	1.31	1.43	1.14	1.13	1.05	1.22	1.22	1.30	1.19	0.13	0.02	0.15

TABLE A3

Adsorption energies in eV of 1/3 ML *OH coadsorbed with 1/3ML *H₂O ($\Delta G_{OH}^{H_2O}$). Avg1 and avg2 are the averages of the solvation energies for group 1 functionals (PBE, PW91) and group 2 functionals (RPBE, vdW and with dispersion corrections) across the same metal. Stdev1/2 are the corresponding standard deviations of avg1/avg2. Avg0 is the average of the solvation energies across the metals for all the functionals and stdev0 is its standard deviation.

metal	PW91	PBE	RPBE	PBE-D3	RPBE-D3	optPBE	BEEF-vdw	avg0	avg1	avg2	stdev0	stdev1	stdev2
Co	0.60	0.53	0.83	0.66	-	0.45	0.64	0.62	0.57	0.65	0.13	0.05	0.16
Rh	0.56	0.58	0.86	0.55	0.54	0.47	0.72	0.61	0.57	0.63	0.13	0.01	0.16
Ir	0.43	0.45	0.76	0.41	0.39	0.34	0.55	0.47	0.44	0.49	0.14	0.01	0.17
Ni	0.70	0.74	0.97	0.65	0.63	0.56	0.72	0.71	0.72	0.70	0.13	0.03	0.16
Pd	0.63	0.65	0.97	0.64	0.63	0.55	0.73	0.69	0.64	0.70	0.14	0.02	0.16
Pt	0.53	0.55	0.78	0.54	0.43	0.46	0.63	0.56	0.54	0.57	0.12	0.02	0.15
Cu	0.94	1.04	1.25	0.97	0.97	0.91	1.09	1.03	0.99	1.04	0.12	0.08	0.14
Ag	1.06	1.11	1.34	1.07	1.03	0.98	1.13	1.10	1.08	1.11	0.12	0.03	0.14
Au	0.80	0.81	1.08	0.79	0.66	0.70	0.89	0.82	0.81	0.82	0.14	0.01	0.17

TABLE A4

Normalized adsorption energies in eV/H₂O molecule of 2/3 ML water adlayer on the Pt NSAs for the different functionals studied ($2 * +2 * \text{H}_2\text{O}(\text{l}) \rightarrow 2 * \text{H}_2\text{O}, \Delta G_{\text{H}_2\text{O}}$).

<i>metal</i>	<i>PW91</i>	<i>PBE</i>	<i>RPBE</i>	<i>PBE-D3</i>	<i>RPBE-D3</i>	<i>optPBE</i>	<i>BEEF-vdw</i>
<i>Co</i>	0.07	0.15	0.24	-0.09	-	-0.01	0.11
<i>Rh</i>	0.10	0.12	0.23	-0.10	-0.01	-0.02	0.08
<i>Ir</i>	0.10	0.12	0.21	-0.10	-0.01	-0.02	0.09
<i>Ni</i>	0.08	0.10	0.23	-0.09	0.00	-0.01	0.13
<i>Pd</i>	0.10	0.13	0.21	-0.10	-0.02	-0.03	0.11
<i>Pt</i>	0.10	0.13	0.24	-0.11	-0.02	-0.03	0.11
<i>Ag</i>	0.09	0.10	0.22	-0.12	-0.02	-0.04	0.10
<i>Au</i>	0.09	0.12	0.23	-0.11	-0.02	-0.03	0.10
<i>Cu</i>	0.12	0.11	0.23	-0.10	-0.03	-0.03	0.09

TABLE A5

Distances in Å between the oxygen of the water lying flat within the 2/3 ML water adlayer and the nearest Pt atom for the different functionals studied.

<i>metal</i>	<i>PW91</i>	<i>PBE</i>	<i>RPBE</i>	<i>PBE-D3</i>	<i>RPBE-D3</i>	<i>optPBE</i>	<i>BEEF-vdw</i>
<i>Co</i>	3.46	3.52	4.26	2.74	-	2.78	3.84
<i>Rh</i>	3.03	3.05	4.38	2.69	2.77	3.00	3.49
<i>Ir</i>	3.00	3.03	4.53	2.62	2.72	2.99	3.49
<i>Ni</i>	3.43	3.47	4.36	2.71	2.77	2.85	3.71
<i>Pd</i>	2.88	2.91	4.64	2.67	2.75	2.98	3.29
<i>Pt</i>	2.82	2.89	4.73	2.66	2.74	2.96	3.26
<i>Ag</i>	3.05	3.10	4.49	2.91	2.89	3.06	3.27
<i>Au</i>	2.97	3.02	4.46	2.79	2.81	2.98	3.21
<i>Cu</i>	3.31	3.32	4.46	2.87	2.85	3.13	3.74

TABLE A6

Distance in Å between the oxygen of the water lying flat in the 1/3 ML *OH coadsorbed with 1/3 ML H₂O and the nearest Pt atom.

<i>metal</i>	<i>PW91</i>	<i>PBE</i>	<i>RPBE</i>	<i>PBE-D3</i>	<i>RPBE-D3</i>	<i>optPBE</i>	<i>BEEF-vdw</i>
<i>Co</i>	2.27	2.27	2.32	2.25	-	2.29	2.34
<i>Rh</i>	2.25	2.25	2.31	2.25	2.28	2.28	2.33
<i>Ir</i>	2.23	2.23	2.28	2.23	2.26	2.26	2.30
<i>Ni</i>	2.27	2.27	2.33	2.27	2.30	2.30	2.35
<i>Pd</i>	2.25	2.26	2.32	2.25	2.29	2.28	2.33
<i>Pt</i>	2.23	2.23	2.28	2.22	2.27	2.25	2.30
<i>Cu</i>	2.34	2.33	2.43	2.32	2.37	2.37	2.46
<i>Ag</i>	2.34	2.35	2.49	2.33	2.40	2.39	2.48
<i>Au</i>	2.28	2.28	2.37	2.27	2.31	2.32	2.40

TABLE A7

Zero point energies (ZPEs) in eV for molecules in the gas phase.

	H ₂ (g)	H ₂ O(g)
PW91	0.269	0.568
PBE	0.268	0.568
RPBE	0.270	0.568
PBE-D3	0.268	0.568
RPBE-D3	0.270	0.567
optPBE	0.271	0.566
BEEF-vdw	0.277	0.577

TABLE A8

Optimized lattice constants (a) in Å for bulk Pt.

Functional	a
PW91	3.99
PBE	3.98
RPBE	4.00
PBE-D3	3.93
RPBE-D3	3.95
optPBE	4.00
BEEF-vdw	4.00

References:

- (1) Calle-Vallejo, F.; Martínez, J. I.; García-Lastra, J. M.; Rossmeisl, J.; Koper, M. T. M. Physical and Chemical Nature of the Scaling Relations between Adsorption Energies of Atoms on Metal Surfaces. *Phys. Rev. Lett.* **2012**, *108* (11), 116103.
- (2) Su, H.-Y.; Sun, K.; Wang, W.-Q.; Zeng, Z.; Calle-Vallejo, F.; Li, W.-X. Establishing and Understanding Adsorption-Energy Scaling Relations with Negative Slopes. *J. Phys. Chem. Lett.* **2016**, *7* (24), 5302-5306.
- (3) He, Z.-D.; Hanselman, S.; Chen, Y.-X.; Koper, M. T. M.; Calle-Vallejo, F. Importance of Solvation for the Accurate Prediction of Oxygen Reduction Activities of Pt-Based Electrocatalysts. *J. Phys. Chem. Lett.* **2017**, *8* (10), 2243-2246.
- (4) Schnur, S.; Groß, A. Properties of Metal-Water Interfaces Studied from First Principles. *New J. Phys.* **2009**, *11* (12), 125003.
- (5) Ogasawara, H.; Brena, B.; Nordlund, D.; Nyberg, M.; Pelmenchikov, A.; Pettersson, L. G. M.; Nilsson, A. Structure and Bonding of Water on Pt(111). *Phys. Rev. Lett.* **2002**, *89* (27), 276102.
- (6) Michaelides, A.; Hu, P. Catalytic Water Formation on Platinum: A First-Principles Study. *J. Am. Chem. Soc.* **2001**, *123* (18), 4235-4242.
- (7) Michaelides, A.; Alavi, A.; King, D. A. Insight into H₂O-Ice Adsorption and Dissociation on Metal Surfaces from First-Principles Simulations. *Phys. Rev. B* **2004**, *69* (11), 113404.

B: Supporting Information for Chapter 3

TABLE B 1

Calculated change in work function $\Delta\phi$, change in surface dipole $\Delta\mu$, distance between surface and adsorbates r , Bader partial charges $|q|$, and free energies of adsorption, of Cl, Br, I, $\text{SO}_4\text{-sol}/\text{SO}_4$ with and without solvation on Pt(111) and Au(111).

adsorbate	$\Delta\phi/ \text{eV}$		$\Delta\mu/ \text{e}\text{\AA}$		$r/ \text{\AA}$		$ q / \text{e-}$		Gads/ eV	
	Pt	Au	Pt	Au	Pt	Au	Pt	Au	Pt	Au
Cl	-0.22	0.40	-0.07	0.13	2.52	2.71	-0.27	-0.39	0.55	0.92
Br	-0.45	0.23	-0.15	0.07	2.63	2.82	-0.12	-0.27	0.18	0.58
I	-0.81	-0.10	-0.27	-0.05	2.72	2.93	0.13	-0.09	-0.52	0.04
SO_4	1.38	2.27	0.47	0.82	2.11	2.22	-0.85	-1.03	0.83	1.51
$\text{SO}_4\text{-sol}$	2.36	3.17	0.79	1.13	2.32	2.51	-0.97	-1.11	0.56	0.82

TABLE B 2

DFT simulated and experimentally measured adsorption potentials¹⁻³ in V vs SHE of I^* , Br^* , Cl^* , and SO_4^* on Pt(111) and Au(111) as well as OH^* and the first and second monolayers of Ag^* on Pt(111). The simulated adsorption potentials include dipole corrections and electrode-electrolyte interfacial field contribution using the experimental PZC of 0.3 and 0.51 V vs SHE for Pt(111) and Au(111).⁴ SO_4^* is solvated by displacing 2 water molecules from a 6 water adsorbed bilayer (leaving 4 water molecules with SO_4^*) and OH^* is solvated by removing a proton from a 3 water cluster (leaving 2 water molecules with OH^*).

adsorbate	Pt(111)		Au(111)	
	DFT	Exp	DFT	Exp
Cl	0.55	0.30	0.92	0.44
Br	0.18	0.12	0.58	0.14
I	-0.52	-0.41	0.04	-0.26
SO_4	0.83	0.48	1.51	0.74
$\text{SO}_4\text{-sol}$	0.56	0.48	0.82	0.74
OH-vac	1.15	0.60	--	--
OH-sol	0.61	0.60	--	--
Ag 1ML	0.99	1.22	--	--
Ag 2ML	0.68	0.77	--	--

TABLE B 3

DFT calculated adsorption potentials, U_{SHE} , with dipole corrections (μ corr) using the experimental PZC of Pt/Au (0.3/0.51 V)⁴ and at PZC = 0 V vs SHE, and without dipole corrections (No μ corr). Diff 1 Pt/Au is the difference between the columns (No μ corr) and (μ corr / PZC Pt/Au, respectively). Diff 2 is the difference between the columns (No μ corr) and (μ corr / PZC=0 V).

Pt(111)					
adsorbate	μ corr / PZC=0.3 V	μ corr / PZC=0 V	No μ corr	Diff 1Pt	Diff2
Cl	0.55	0.54	0.55	0.01	0.01
Br	0.18	0.17	0.18	-0.01	0.01
I	-0.52	-0.54	-0.59	-0.07	-0.05
SO ₄	0.83	0.86	0.79	-0.04	-0.07
SO ₄ -sol	0.56	0.60	0.54	-0.03	-0.06
OH vac	1.15	1.15	1.14	-0.01	-0.01
OH-sol	0.61	0.59	0.63	0.02	0.04
Ag 1ML	0.99	0.99	0.97	-0.01	-0.01
Ag 2ML	0.68	0.68	0.68	0.00	0.00
Au(111)					
	μ corr / PZC=0.51 V	μ corr / PZC=0 V	No μ corr	Diff 1Au	Diff2
Cl	0.92	0.94	0.90	-0.02	-0.04
Br	0.58	0.59	0.58	0.00	-0.01
I	0.04	0.03	0.03	-0.01	0.00
SO ₄	1.51	1.58	1.37	-0.14	-0.22
SO ₄ -sol	0.82	0.91	0.78	-0.05	-0.13

References:

- (1) Garcia-Araez, N.; Climent, V.; Herrero, E.; Feliu, J.; Lipkowski, J. Thermodynamic Studies of Bromide Adsorption at the Pt(111) Electrode Surface Perchloric Acid Solutions: Comparison with Other Anions. *J. Electroanal. Chem.* **2006**, 591 (2), 149-158.
- (2) Lipkowski, J.; Shi, Z.; Chen, A.; Pettinger, B.; Bilger, C. Ionic Adsorption at the Au(111) Electrode. *Electrochimica Acta* **1998**, 43 (19), 2875-2888.
- (3) Hachiya, T.; Itaya, K. In Situ Scanning Tunneling Microscopy of Underpotential Deposition in Aqueous Solution III. Silver Adlayers on Au(111). *Ultramicroscopy* **1992**, 42-44, 445-452.
- (4) Ojha, K.; Arulmozhi, N.; Aranzales, D.; Koper, M. T. M. Double Layer at the Pt(111)-Aqueous Electrolyte Interface: Potential of Zero Charge and Anomalous Gouy-Chapman Screening. *Angew. Chem. Int. Ed.* **2020**, 59 (2), 711-715.

C: Supporting Information for Chapter 4

C.1 P SLANE-WAVE CUTOFF CONVERGENCE TEST	142
C.2 DATA SET A.....	142
C.3 DATA SET B	144
C.4 PINPOINTING ERRORS	147
C.4.1 PBE.....	149
C.4.1.1. -CH _x ERRORS IN PBE.....	149
C.4.1.2. -C=O- ERRORS IN PBE.....	150
C.4.1.3. -(C=O)O- ERRORS IN PBE.....	151
C.4.1.4. -OH ERRORS IN PBE.....	152
C.4.2. PW91	153
C.4.2.1. -CH _x IN PW91	153
C.4.2.2. -C=O- IN PW91	153
C.4.2.3. -(C=O)O- ERRORS IN PW91	154
C.4.2.4. -OH ERRORS IN PW91.....	154
C.4.3. RPBE.....	155
C.4.3.1. -CH _x ERRORS IN RPBE	155
C.4.3.2. -C=O- ERRORS IN RPBE	155
C.4.3.3. -(C=O)O- ERRORS IN RPBE	156
C.4.3.4. -OH ERRORS IN RPBE	156
C.4.4. BEEF-vdW.....	157
C.4.4.1. -CH _x ERRORS IN BEEF-vdW	157
C.4.4.2. -C=O- ERRORS IN BEEF-vdW.....	157
C.4.4.3. -(C=O)O- ERRORS IN BEEF-vdW	158
C.4.4.4. -OH ERRORS IN BEEF-vdW	159
C.4.4.5. H ₂ ERRORS IN BEEF-vdW.....	159
C.5 ELECTROCATALYSIS-RELATED DATA	161
C.6 INTERLAYER COHESIVE ENERGY IN GRAPHITE	165
C.7 ALTERNATIVE ANALYSIS USING TRAINING AND EXTRAPOLATION SETS	165
C.8 REFERENCES	172

C.1 Plane-wave cutoff convergence test

Table C1 shows the results of a plane-wave cutoff test made to ensure that the results provided here do not strongly depend on the use of plane waves as a basis set and that 400 eV suffices to provide converged results.

TABLE C1

Plane-wave energy cutoff test ($ENCUT$, in eV) as for PBE, based on the free energy (ΔG_{DFT} , in eV) of $\text{CO}_2 + \text{H}_2 \rightarrow \text{CO} + \text{H}_2\text{O}$ from 300 eV to 1000 eV. The values under Diff (in eV) are the difference between successive higher and smaller plane-wave energy cutoffs.

$ENCUT$	ΔG_{DFT}	$Diff$
300	0.74	
350	0.73	-1.10×10^{-2}
400	0.73	-2.46×10^{-3}
500	0.74	1.17×10^{-2}
600	0.74	-4.07×10^{-4}
700	0.71	-3.18×10^{-2}
800	0.72	1.69×10^{-2}
900	0.71	-1.54×10^{-2}
1000	0.70	-3.66×10^{-3}

C.2 Data set A

In Table C2 we provide the calculated and experimental formation energies of the 27 compounds under study. The energies are calculated with respect to $\text{H}_2(\text{g})$, $\text{O}_2(\text{g})$, and $\text{C}(\text{s})$, modelled as graphene (see section 6). $\text{O}_2(\text{g})$ energetics was corrected to obtain the values in Table C2, as its poor description by most xc-functionals is well known.¹ The semiempirical approach is based on $\text{H}_2(\text{g})$, $\text{H}_2\text{O}(\text{l})$, and the energetics of $2\text{H}_2 + \text{O}_2 \rightarrow 2\text{H}_2\text{O}$, as described in previous works.^{1-4,3} For PBE, the gas-phase correction is -0.46 eV. If that correction is not applied, the average deviation in Data set A from experiments is 0.21 eV for PBE and all deviations are positive, corroborating previous observations on formation energies in which diatomic molecules are involved.⁴

TABLE C2

Standard free energies of formation ($\Delta G_{\text{DFT}}^\circ$, in eV) for 27 gas-phase molecules calculated with PBE, PW91, RPBE, and BEEF-vdW xc-functionals, together with the corresponding experimental values from thermodynamic tables.⁵⁻⁷

<i>Compound</i>	<i>PBE</i>	<i>PW91</i>	<i>RPBE</i>	<i>BEEF-vdW</i>	<i>exp</i>
CO	-1.18	-1.17	-1.50	-1.60	-1.42
CO ₂	-4.27	-4.23	-4.55	-4.65	-4.09
CH ₂ O (<i>formaldehyde</i>)	-1.13	-1.14	-1.27	-1.27	-1.06
CH ₄ (<i>methane</i>)	-0.51	-0.55	-0.46	-0.27	-0.52
CH ₄ O (<i>methanol</i>)	-1.72	-1.75	-1.67	-1.59	-1.68
CH ₂ O ₂ (<i>formic acid</i>)	-3.83	-3.82	-3.92	-3.98	-3.64
C ₂ H ₂ O ₂ (<i>glyoxal</i>)	-2.13	-2.14	-2.39	-2.46	-1.97
C ₂ H ₄ O ₂ (<i>acetic acid</i>)	-4.03	-4.05	-4.04	-4.02	-3.88
C ₂ H ₄ O ₂ (<i>methyl formate</i>)	-3.31	-3.34	-3.34	-3.36	-3.11
C ₂ H ₄ (<i>ethylene</i>)	0.75	0.69	0.68	0.88	0.71
C ₂ H ₄ O (<i>ethylene oxide</i>)	-0.31	-0.32	-0.34	-0.19	-0.13
C ₂ H ₄ O (<i>acetaldehyde</i>)	-1.46	-1.50	-1.53	-1.42	-1.38
C ₂ H ₆ (<i>ethane</i>)	-0.29	-0.36	-0.21	0.08	-0.33
C ₂ H ₆ O (<i>ethanol</i>)	-1.74	-1.80	-1.63	-1.47	-1.74
C ₂ H ₆ O (<i>dimethyl ether</i>)	-1.21	-1.27	-1.10	-0.97	-1.17
C ₂ H ₂ (<i>acetylene</i>)	2.29	2.25	2.06	2.21	2.18
C ₃ H ₈ (<i>propane</i>)	-0.17	-0.26	-0.01	0.34	-0.24
C ₃ H ₆ O (<i>acetone</i>)	-1.65	-1.71	-1.64	-1.45	-1.58
C ₃ H ₈ O (<i>isopropanol</i>)	-1.73	-1.81	-1.52	-1.30	-1.80
C ₃ H ₈ O (<i>propanol</i>)	-1.61	-1.69	-1.41	-1.18	-1.66
C ₃ H ₆ O (<i>propanal</i>)	-1.36	-1.42	-1.35	-1.18	-1.28
C ₃ H ₆ O (<i>propylene oxide</i>)	-0.43	-0.46	-0.38	-0.16	-0.29
C ₃ H ₆ O ₂ (<i>methyl acetate</i>)	-3.51	-3.56	-3.46	-3.40	-3.39
C ₄ H ₈ O (<i>butanal</i>)	-1.19	-1.27	-1.13	-0.88	-1.18
C ₄ H ₁₀ (<i>butane</i>)	-0.05	-0.16	0.18	0.59	-0.19
C ₄ H ₁₀ O (<i>butanol</i>)	-1.48	-1.58	-1.22	-0.93	-1.56
C ₅ H ₁₂ (<i>pentane</i>)	0.09	-0.06	0.38	0.85	-0.09

C.3 Data set B

In the following tables we provide the reaction energies calculated for the formation of molecules in data set A from CO₂ (Table C3) and CO (Table C4). In the free energies of reaction in Tables C3 and C4, we used gas-phase water, H₂O(g).

TABLE C3

Data set containing free energies of reaction (in eV) for the PBE, PW91, RPBE, BEEF-vdW xc-functionals together with the corresponding experimental values. The data set contains the free energies of reaction from CO₂(g) and H₂(g) and producing the specific substance in parentheses and H₂O(g), when needed.

Reaction	PBE	PW91	RPBE	BEEF-vdW	Exp
CO ₂ + H ₂ → CO + H ₂ O	0.73	0.69	0.68	0.68	0.30
CO ₂ + H ₂ → HCOOH	0.45	0.41	0.63	0.67	0.45
CO ₂ + 2 H ₂ → CH ₂ O + H ₂ O (formaldehyde)	0.78	0.73	0.91	1.01	0.66
CO ₂ + 3 H ₂ → CH ₃ OH + H ₂ O (methanol)	0.18	0.11	0.51	0.69	0.04
CO ₂ + 4 H ₂ → CH ₄ + 2 H ₂ O (methane)	-0.97	-1.05	-0.65	-0.36	-1.17
2 CO ₂ + 6 H ₂ → C ₂ H ₄ + 4 H ₂ O (ethylene)	-0.18	-0.32	0.30	0.70	-0.59
2 CO ₂ + 3 H ₂ → C ₂ H ₂ O ₂ + 2 H ₂ O (glyoxal)	1.68	1.59	1.97	2.10	1.47
2 CO ₂ + 4 H ₂ → C ₂ H ₄ O ₂ + 2 H ₂ O (acetic acid)	-0.22	-0.32	0.32	0.54	-0.44
2 CO ₂ + 4 H ₂ → C ₂ H ₄ O ₂ + 2 H ₂ O (methyl formate)	0.50	0.39	1.02	1.19	0.33
2 CO ₂ + 5 H ₂ → C ₂ H ₄ O + 3 H ₂ O (eth. oxide)	1.13	1.04	1.65	2.00	0.93
2 CO ₂ + 5 H ₂ → C ₂ H ₄ O + 3 H ₂ O (acetaldehyde)	-0.02	-0.14	0.46	0.77	-0.31
2 CO ₂ + 5 H ₂ → C ₂ H ₂ + 4 H ₂ O (acetylene)	1.37	1.24	1.68	2.02	0.87
2 CO ₂ + 6 H ₂ → C ₂ H ₆ O + 3 H ₂ O (ethanol)	-0.30	-0.44	0.36	0.72	-0.67
2 CO ₂ + 6 H ₂ → C ₂ H ₆ O + 3 H ₂ O (dimethyl ether)	0.23	0.09	0.89	1.22	-0.10
2 CO ₂ + 7 H ₂ → C ₂ H ₆ + 4 H ₂ O (ethane)	-1.22	-1.37	-0.58	-0.10	-1.63
3 CO ₂ + 8 H ₂ → C ₃ H ₆ O + 5 H ₂ O (acetone)	-0.68	-0.86	0.16	0.65	-1.17
3 CO ₂ + 9 H ₂ → C ₃ H ₈ O + 5 H ₂ O (isopropanol)	-0.75	-0.96	0.29	0.80	-1.38
3 CO ₂ + 10 H ₂ → C ₃ H ₈ + 6 H ₂ O (propane)	-1.56	-1.77	-0.58	0.07	-2.20
3 CO ₂ + 9 H ₂ → C ₃ H ₈ O + 5 H ₂ O (1-propanol)	-0.63	-0.83	0.39	0.91	-1.24
3 CO ₂ + 8 H ₂ → C ₃ H ₆ O + 3 H ₂ O (propanal)	-0.38	-0.56	0.45	0.92	-0.87
3 CO ₂ + 8 H ₂ → C ₃ H ₆ O + 5 H ₂ O (propylene oxide)	0.55	0.39	1.42	1.93	0.13
3 CO ₂ + 7 H ₂ → C ₃ H ₆ O ₂ + 4 H ₂ O (methyl acetate)	-0.17	-0.34	0.71	1.06	-0.60
4 CO ₂ + 11 H ₂ → C ₄ H ₈ O + 7 H ₂ O (butanal)	-0.67	-0.92	0.49	1.12	-1.42
4 CO ₂ + 13 H ₂ → C ₄ H ₁₀ + 8 H ₂ O (butane)	-1.91	-2.18	-0.58	0.23	-2.79
4 CO ₂ + 12 H ₂ → C ₄ H ₁₀ O + 7 H ₂ O (1-butanol)	-0.96	-1.23	0.39	1.07	-1.79
5 CO ₂ + 16 H ₂ → C ₅ H ₁₂ + 10 H ₂ O (pentane)	-2.24	-2.58	-0.56	0.40	-3.34

TABLE C4

Data set containing free energies of reaction (in eV) for the PBE, PW91, RPBE, BEEF-vdW xc-functionals together with the corresponding experimental values. The table contains free energies of reaction from CO(g) and H₂(g) and producing the specific substance in parentheses and H₂O(g), when needed. Only for formic acid, the product is obtained from CO(g) and H₂O(g).

<i>Reaction</i>	<i>PBE</i>	<i>PW91</i>	<i>RPBE</i>	<i>BEEF-vdW</i>	<i>Exp</i>
$CO + H_2O \rightarrow CO_2 + H_2$	-0.73	-0.69	-0.68	-0.68	-0.30
$CO + H_2O \rightarrow HCOOH$ (<i>formic acid</i>)	-0.28	-0.28	-0.05	-0.01	0.15
$CO + H_2 \rightarrow CH_2O$ (<i>formaldehyde</i>)	0.05	0.03	0.23	0.33	0.36
$CO + 2H_2 \rightarrow CH_3OH$ (<i>methanol</i>)	-0.54	-0.58	-0.18	0.01	-0.26
$CO + 3H_2 \rightarrow CH_4 + H_2O$ (<i>methane</i>)	-1.70	-1.74	-1.33	-1.04	-1.47
$2 CO + 4 H_2 \rightarrow C_2H_4 + 2 H_2O$ (<i>ethylene</i>)	-1.63	-1.71	-1.07	-0.65	-1.19
$2 CO + H_2 \rightarrow C_2H_2O_2$ (<i>glyoxal</i>)	0.23	0.21	0.60	0.74	0.88
$2 CO + 2 H_2 \rightarrow C_2H_4O_2$ (<i>acetic acid</i>)	-1.67	-1.71	-1.05	-0.82	-1.03
$2 CO + 2 H_2 \rightarrow C_2H_4O_2$ (<i>methyl formate</i>)	-0.95	-1.00	-0.35	-0.16	-0.26
$2 CO + 3 H_2 \rightarrow C_2H_4O + H_2O$ (<i>eth. oxide</i>)	-0.32	-0.35	0.28	0.64	0.34
$2 CO + 3 H_2 \rightarrow C_2H_4O + H_2O$ (<i>acetaldehyde</i>)	-1.48	-1.53	-0.91	-0.59	-0.90
$2 CO + 3H_2 \rightarrow C_2H_2 + 2 H_2O$ (<i>acetylene</i>)	-0.09	-0.15	0.31	0.67	0.28
$2 CO + 4 H_2 \rightarrow C_2H_6O + H_2O$ (<i>ethanol</i>)	-1.75	-1.82	-1.01	-0.64	-1.27
$2 CO + 4 H_2 \rightarrow C_2H_6O + H_2O$ (<i>dimethyl ether</i>)	-1.22	-1.30	-0.48	-0.13	-0.69
$2 CO + 5 H_2 \rightarrow C_2H_6 + 2 H_2O$ (<i>ethane</i>)	-2.67	-2.75	-1.95	-1.46	-2.23
$3 CO + 5 H_2 \rightarrow C_3H_6O + 2 H_2O$ (<i>acetone</i>)	-2.86	-2.94	-1.89	-1.39	-2.06
$3 CO + 6 H_2 \rightarrow C_3H_8O + 2 H_2O$ (<i>isopropanol</i>)	-2.93	-3.03	-1.77	-1.24	-2.27
$3 CO + 7 H_2 \rightarrow C_3H_8 + 3 H_2O$ (<i>propane</i>)	-3.74	-3.85	-2.63	-1.97	-3.08
$3 CO + 6 H_2 \rightarrow C_3H_8O + 2 H_2O$ (<i>propanol</i>)	-2.81	-2.91	-1.66	-1.12	-2.16
$3 CO + 5 H_2 \rightarrow C_3H_6O + 2 H_2O$ (<i>1-propanal</i>)	-2.56	-2.64	-1.60	-1.11	-1.77
$3 CO + 5 H_2 \rightarrow C_3H_6O + 2 H_2O$ (<i>propylene oxide</i>)	-1.63	-1.69	-0.63	-0.10	-1.01
$3 CO + 4 H_2 \rightarrow C_3H_6O_2 + H_2O$ (<i>methyl acetate</i>)	-2.35	-2.42	-1.34	-0.97	-1.49
$4 CO + 7 H_2 \rightarrow C_4H_8O + 3 H_2O$ (<i>butanal</i>)	-3.58	-3.69	-2.25	-1.59	-2.60
$4 CO + 9 H_2 \rightarrow C_4H_{10} + 4 H_2O$ (<i>butane</i>)	-4.81	-4.95	-3.31	-2.48	-3.98
$4 CO + 8 H_2 \rightarrow C_4H_{10}O + 3 H_2O$ (<i>1-butanol</i>)	-3.87	-4.00	-2.34	-1.64	-2.98
$5 CO + 11 H_2 \rightarrow C_5H_{12} + 5 H_2O$ (<i>pentane</i>)	-5.87	-6.05	-3.98	-2.99	-4.82

In Table C5 we list the corrections included for all analyzed compounds depending on the functional used.

TABLE C5

Applied corrections per functional for the molecules in data set A.

<i>Compound</i>	<i>PBE</i>	<i>PW91</i>	<i>RPBE</i>	<i>BEEF-vdW</i>
CO	CO	CO	CO	CO
CO ₂	CO ₂	CO ₂	CO ₂	CO ₂
CH ₂ O (<i>formaldehyde</i>)	-C=O-	-C=O-	-C=O-	-C=O-
CH ₄ (<i>methane</i>)	-CHx	-	-CHx	-CHx
CH ₄ O (<i>methanol</i>)	-CHx	-	-CHx	-CHx, OH
CH ₂ O ₂ (<i>formic acid</i>)	CO ₂	-(C=O)O-	-(C=O)O-	-(C=O)O-
C ₂ H ₂ O ₂ (<i>glyoxal</i>)	2 -C=O-	2 -C=O-	2 -C=O-	2 -C=O-
C ₂ H ₄ O ₂ (<i>acetic acid</i>)	-CHx, CO ₂	-(C=O)O-	-CHx, -(C=O)O-	-CHx, -(C=O)O-
C ₂ H ₄ O ₂ (<i>methyl formate</i>)	-CHx, CO ₂	-(C=O)O-	-CHx, -(C=O)O-	-CHx, -(C=O)O-
C ₂ H ₄ (<i>ethylene</i>)	-	-	-	-
C ₂ H ₄ O (<i>ethylene oxide</i>)	-	-	-	-
C ₂ H ₄ O (<i>acetaldehyde</i>)	-CHx, -C=O-	-C=O-	-CHx, -C=O-	-CHx, -C=O-
C ₂ H ₆ (<i>ethane</i>)	2 -CHx	-	2 -CHx	2 -CHx
C ₂ H ₆ O (<i>ethanol</i>)	2 -CHx	-	2 -CHx	2 -CHx, OH
C ₂ H ₆ O (<i>dimethyl ether</i>)	-	-	-	-
C ₂ H ₂ (<i>acetylene</i>)	-	-	-	-
C ₃ H ₈ (<i>propane</i>)	3-CHx	-	3-CHx	3-CHx
C ₃ H ₆ O (<i>acetone</i>)	2 -CHx, -C=O-	-C=O-	2 -CHx, -C=O-	2 -CHx, -C=O-
C ₃ H ₈ O (<i>isopropanol</i>)	3-CHx	-	3-CHx	3 -CHx, OH
C ₃ H ₈ O (<i>propanol</i>)	3-CHx	-	3-CHx	3 -CHx, OH
C ₃ H ₆ O (<i>propanal</i>)	2 -CHx, -C=O-	-C=O-	2 -CHx, -C=O-	2 -CHx, -C=O-
C ₃ H ₆ O (<i>propylene oxide</i>)	-CHx	-	-CHx	-CHx
C ₃ H ₆ O ₂ (<i>methyl acetate</i>)	2 -CHx, CO ₂	-(C=O)O-	2 -CHx, -(C=O)O-	2 -CHx, -(C=O)O-
C ₄ H ₈ O (<i>butanal</i>)	3 -CHx, -C=O-	-C=O-	3 -CHx, -C=O-	3 -CHx, -C=O-
C ₄ H ₁₀ (<i>butane</i>)	4 -CHx	-	4 -CHx	4 -CHx
C ₄ H ₁₀ O (<i>butanol</i>)	4 -CHx	-	4 -CHx	4 -CHx, OH
C ₅ H ₁₂ (<i>pentane</i>)	5 -CHx	-	5 -CHx	5 -CHx

C.4 Pinpointing errors

For all functionals, the errors in the energies of CO and CO₂ are determined by means of Eq. 4.2 in the main text. In the following, we summarize how the other errors in Table 1, besides \mathcal{E}_{CO} and \mathcal{E}_{CO_2} , were determined for each functional. The general procedure is shown in the workflow scheme 4.1 in the main text, and below.

1. Start with the simplest organic functional group in the data set. In this case, we start with alkanes, which are formed only by -CH_x groups (see the column highlighted in red in Figure C1).

n_C		ΔG_{DFT}°	ΔG_{EXP}°	ε_T	ε_T/n_C
1	CH ₄	-0.51	-0.52	0.02	0.02
2	C ₂ H ₆	-0.29	-0.33	0.04	0.02
3	C ₃ H ₈	-0.17	-0.24	0.07	0.02
4	C ₄ H ₁₀	-0.05	-0.19	0.14	0.03
5	C ₅ H ₁₂	0.09	-0.09	0.17	0.03
				avg	0.03
				stdev	0.01

FIGURE C1

Pinpointing errors in data set A. Step 1: the alkanes in the set are gathered.

2. Calculate ε_T (Eq. 4.2 in the main text) and find common trends (is the error constant or increasing/decreasing by a relatively constant amount?). In this case for PBE, the error increases alongside the length of the carbon chain n_C (see the column highlighted in red in Figure C2).

n_C		ΔG_{DFT}°	ΔG_{EXP}°	ϵ_T	ϵ_T/n_C
1	CH ₄	-0.51	-0.52	0.02	0.02
2	C ₂ H ₆	-0.29	-0.33	0.04	0.02
3	C ₃ H ₈	-0.17	-0.24	0.07	0.02
4	C ₄ H ₁₀	-0.05	-0.19	0.14	0.03
5	C ₅ H ₁₂	0.09	-0.09	0.17	0.03
				avg	0.03
				stdev	0.01

FIGURE C2

Pinpointing errors in data set A. Step 2: the errors are calculated for each substance in the list.

3. To find an approximate ϵ_{CH_x} , normalize the separate errors by the number of -CH_x units (n_C) and calculate the average (see the column highlighted in red in Figure C3).

n_C		ΔG_{DFT}°	ΔG_{EXP}°	ϵ_T	ϵ_T/n_C
1	CH ₄	-0.51	-0.52	0.02	0.02
2	C ₂ H ₆	-0.29	-0.33	0.04	0.02
3	C ₃ H ₈	-0.17	-0.24	0.07	0.02
4	C ₄ H ₁₀	-0.05	-0.19	0.14	0.03
5	C ₅ H ₁₂	0.09	-0.09	0.17	0.03
				avg	0.03
				stdev	0.01

FIGURE C3

Pinpointing errors in data set A. Step 3: the errors are normalized by the number of -CH_x units in the compound. The -CH_x error is the average of all the individual errors in the list.

4. For molecules with more than one functional group, first eliminate the error contribution of a known \mathcal{E}_i , then obtain the average value of the isolated error. For example, for aldehydes and ketones the carbonyl-group error is isolated by subtracting from the total error the contribution of the hydrocarbon error (see the column highlighted in red in Figure C4).

	ΔG_{DFT}°	ΔG_{EXP}°	\mathcal{E}_T	$\mathcal{E}_T - n_C \cdot \mathcal{E}_{CH_x}$
CH ₂ O Formaldehyde	-1.13	-1.06	-0.06	-0.06
C ₂ H ₄ O Acetaldehyde	-1.46	-1.38	-0.09	-0.11
C ₃ H ₆ O Propanal	-1.36	-1.28	-0.08	-0.13
C ₄ H ₈ O Butanal	-1.19	-1.18	0.00	-0.08
C ₃ H ₆ O Acetone	-1.65	-1.58	-0.07	-0.12
			avg	-0.10
			stdev	0.03

FIGURE C4

Pinpointing errors in data set A. Step 4: the aldehydes in the data set are gathered, their errors calculated and the -CH_x errors subtracted to ultimately find the carbonyl-related error upon averaging.

To isolate the contributions of the groups to the overall errors, at least 2 molecules representative of the organic functional group are necessary. To illustrate that, the error in the carbonyl group -C=O- for PW91 was determined using 4 representative molecules out of 5, see Table C10.

C.4.1 PBE

C.4.1.1 -CH_x errors in PBE

To determine whether there is an error on this functional group we took the alkanes in data set A and compared their associated errors calculated with Eq. 4.2 in the main text. The errors are shown in Table C6.

The first observation is that the absolute value of \mathcal{E}_T increases alongside the length of the carbon chain. Thus, the error is normalized by the number of carbon atoms in the molecule, as shown in Table C6 in the column \mathcal{E}_T / n_C . The average of those values is the error attributed to -CH_x components. As this is a

cumulative error, it is particularly important to take it into account when correcting energies of molecules with large carbon chains.

TABLE C6

Calculated (PBE) and experimental standard free energies in eV for the alkanes in data set A. ϵ_T is the error with respect to experiments (Eq. 4.2 in the main text), ϵ_T/n_C is the error normalized by the number of $-\text{CH}_x$ moieties (n_C) in the molecule. The average of ϵ_T/n_C is equivalent to ϵ_{CH_x} in Table 1 of the main text.

$-\text{CH}_x$		$\Delta G_{\text{DFT}}^\circ$	$\Delta G_{\text{EXP}}^\circ$	ϵ_T	ϵ_T/n_C
1	CH ₄	-0.51	-0.52	0.02	0.02
2	C ₂ H ₆	-0.29	-0.33	0.04	0.02
3	C ₃ H ₈	-0.17	-0.24	0.07	0.02
4	C ₄ H ₁₀	-0.05	-0.19	0.14	0.03
5	C ₅ H ₁₂	0.09	-0.09	0.17	0.03
				avg	0.03
				stdev	0.01

C.4.1.2. -C=O- errors in PBE

-C=O- is the error of carbonyl groups, so it pertains to aldehydes and ketones. Some of the molecules in this group contain $-\text{CH}_x$ moieties, so to determine the error that comes solely from the carbonyl group we subtract the $-\text{CH}_x$ error from the total error, as shown in Table C7 under $\epsilon_T - n_C \cdot \epsilon_{\text{CH}_x}$. Acetaldehyde has one $-\text{CH}_x$ moiety, propanal and acetone have two, and butanal has three. The average of the remainders ($\epsilon_T - n_C \cdot \epsilon_{\text{CH}_x}$) is the error for carbonyl groups, which is equal to -0.1 eV. To determine whether this error is significant and should be considered apart from the CO error, we took the difference between the calculated average error ($\epsilon_{-\text{C}=\text{O}-}$) and ϵ_T^{CO} (0.24 eV). As the difference is on average -0.35 eV, we can safely classify the -C=O- error in a separate category and, thus, carbonyl groups are to be corrected by ~ -0.1 eV.

TABLE C7

Calculated (PBE) and experimental standard free energies in eV for the molecules with carbonyl groups in data set A. $\varepsilon_T - n_C \cdot \varepsilon_{CH_x}$ is the difference between the respective error and the number of $-CH_x$ components in the molecule. The average error corresponds to the $-C=O-$ error in Table 1 of the main text.

<i>aldehydes/ketones</i>	ΔG_{DFT}°	ΔG_{EXP}°	ε_T	$\varepsilon_T - n_C \cdot \varepsilon_{CH_x}$
Formaldehyde	-1.13	-1.06	-0.06	-0.06
Acetaldehyde	-1.46	-1.38	-0.09	-0.11
Propanal	-1.36	-1.28	-0.08	-0.13
Butanal	-1.19	-1.18	0.00	-0.08
Acetone	-1.65	-1.58	-0.07	-0.12
			avg	-0.10
			stdev	0.03

C.4.1.3. $-(C=O)O-$ errors in PBE

A similar analysis to that of $-C=O-$ is followed for carboxylic acids and esters in data set A. First, we find that ε_T is nearly constant for all the molecules containing the $-(C=O)O-$ moiety, then the error from $-CH_x$ is subtracted to finally obtain the tabulated error contribution for $-(C=O)O-$ moieties of -0.19 eV. Furthermore, the difference in the calculated error and the CO_2 error is ~ -0.01 eV, indicating that the error in the energies of carboxyl-containing molecules might be corrected by the CO_2 error, depending on the desired level of accuracy.

TABLE C8

Calculated (PBE) and experimental standard free energies in eV for carboxylic acids and esters in data set A. Avg is the average error associated to these compounds.

<i>acids/esters</i>	ΔG_{DFT}°	ΔG_{EXP}°	ε_T	$\varepsilon_T - n_C \cdot \varepsilon_{CH_x}$
Formic Acid	-3.83	-3.64	-0.19	-0.19
Acetic Acid	-4.03	-3.88	-0.15	-0.18
Methyl formate	-3.31	-3.11	-0.20	-0.23
Metyl Acetate	-3.51	-3.39	-0.13	-0.18
			avg	-0.19
			stdev	0.02

C.4.1.4. -OH errors in PBE

To determine whether alcohols need a correction, we deconvoluted the total error and the $-CH_x$ error. The average error for -OH moieties is -0.04 eV. The MAE on the products from CO_2 and H_2 reactions, with and without correction -OH is 0.037 and 0.040 eV. For products from CO and H_2 , the MAE with and without correction for -OH is 0.035 and 0.034 eV. Hence, we do not correct -OH, but note that this correction can enhance the reaction energetics particularly for short carbon chain alcohols, such as methanol and ethanol.

For example, the error for producing methanol within PBE based on the reaction $CO_2 + 3H_2 \rightarrow CH_3OH + H_2O$ is 0.14 eV, as seen from Table C3, data set B. After correcting the free energy of CO_2 on the reactants and $-CH_x$ on the products (Eq. 4.6 in the main text: $\Delta G_{DFT}^{\circ} - \varepsilon_{CO_2} + \varepsilon_{CH_x}$) as (0.18 eV + (-0.19 eV) - (0.03 eV)), the free energy becomes $\Delta G_{corr}^{\circ} = -0.04$ eV and the error is -0.08 eV. Further correction by $\varepsilon_{OH} = -0.04$ eV, reduces the error to -0.04 eV.

TABLE C9

Calculated (PBE) and standard free energies in eV for alcohols in data set A. Avg is the average error associated to these compounds.

<i>alcohol</i>	ΔG_{DFT}°	ΔG_{EXP}°	ε_T	$\varepsilon_T - n_C \cdot \varepsilon_{CH_x}$
Methanol	-1.72	-1.68	-0.04	-0.06
Ethanol	-1.74	-1.74	0.00	-0.05
Propanol	-1.61	-1.66	0.05	-0.03
Butanol	-1.48	-1.56	0.09	-0.02
			avg	-0.04
			stdev	0.02

C.4.2. PW91

C.4.2.1. -CH_x in PW91

As shown in Table C10, -CH_x moieties in PW91 do not show significant errors. Therefore, PW91 calculated energies do not require this type of correction.

TABLE C10

Calculated (PW91) and experimental standard free energies in eV for the alkanes in data set A and an assessment of their associated errors.

<i>-CH_x</i>		ΔG_{DFT}°	ΔG_{EXP}°	ε_T	ε_T / n_C
1	CH ₄	-0.55	-0.52	-0.02	-0.02
2	C ₂ H ₆	-0.36	-0.33	-0.03	-0.01
3	C ₃ H ₈	-0.26	-0.24	-0.02	-0.01
4	C ₄ H ₁₀	-0.16	-0.19	0.03	0.01
5	C ₅ H ₁₂	-0.06	-0.09	0.03	0.01
				avg	-0.01
				stdev	0.01

C.4.2.2. -C=O- in PW91

As there is practically no error associated to -CH_x moieties for PW91, the errors for carbonyl groups are determined directly from the differences with respect to experiments.

TABLE C11

Calculated (PW91) and experimental standard free energies in eV for aldehydes and ketones in data set A, and an assessment of their average associated errors.

<i>aldehydes/ketones</i>	ΔG_{DFT}°	ΔG_{EXP}°	ε_T
Formaldehyde	-1.14	-1.06	-0.07
Acetaldehyde	-1.50	-1.38	-0.12
Propanal	-1.42	-1.30	-0.12
Butanal	-1.27	-1.18	-0.09
		avg	-0.10
		stdev	0.02

C.4.2.3. $-(C=O)O-$ errors in PW91

In line with PBE, the error for acids and esters in PW91 is similar to the CO_2 error. In fact, the average error of -0.19 eV differs from that of CO_2 (-0.15 eV) by 0.05 eV. In both cases, for the products obtained from CO_2 and H_2 , and CO and H_2 , the MAE is 0.041 and 0.037 eV correcting by -0.15 and -0.19 eV, respectively. Here we have decided to correct the $-(C=O)O-$ moiety by the error found (-0.19 eV) but, in principle, one could correct CO_2 , carboxylic acids and esters using the CO_2 error, depending on the required degree of accuracy.

TABLE C12

Calculated (PW91) and experimental standard free energies of formation in eV for carboxylic acids and esters in data set A, and an assessment of their associated errors.

<i>acids/esters</i>	ΔG_{DFT}°	ΔG_{EXP}°	ϵ_T
Formic Acid	-3.82	-3.64	-0.18
Acetic Acid	-4.05	-3.88	-0.17
Methyl formate	-3.34	-3.11	-0.23
Methyl Acetate	-3.56	-3.39	-0.18
		avg	-0.19
		stdev	0.03

C.4.2.4. $-OH$ errors in PW91

Based on the error analysis in Table C10, this functional does not display sizable $-CH_x$ errors. Therefore, the average $-OH$ error can be straightforwardly calculated in Table C13 as -0.04 eV. As is the case for PBE (section C.4.1.4), correcting this error might be advisable for short carbon chain alcohols, depending on the required accuracy. The MAE for CO_2 and H_2 products and for CO and H_2 (some using CO and H_2O) is 0.036 and 0.037 eV with and without $-OH$ correction.

TABLE C13

Calculated (PW91) and experimental standard free energies in eV for alcohols in data set A, and an assessment of their associated errors.

<i>alcohol</i>	ΔG_{DFT}°	ΔG_{EXP}°	ϵ_T
Methanol	-1.75	-1.68	-0.07
Ethanol	-1.80	-1.74	-0.06
Propanol	-1.69	-1.68	-0.01
Butanol	-1.58	-1.56	-0.02
		avg	-0.04
		stdev	0.03

C.4.3. RPBE

C.4.3.1. -CH_x errors in RPBE

The average contribution of -CH_x moieties to the total errors in the formation energies of alkanes is 0.08 eV/CH_x. The total error is, thus, appreciably larger than that of PBE for large molecules.

TABLE C14

Calculated (RPBE) and experimental standard free energies in eV for the alkanes in data set A, and an assessment of their associated errors.

<i>-CH_x</i>		ΔG_{DFT}°	ΔG_{EXP}°	ϵ_T	ϵ_T/n_C
1	CH ₄	-0.46	-0.52	0.07	0.07
2	C ₂ H ₆	-0.21	-0.33	0.13	0.06
3	C ₃ H ₈	-0.01	-0.24	0.23	0.08
4	C ₄ H ₁₀	0.18	-0.19	0.37	0.09
5	C ₅ H ₁₂	0.38	-0.09	0.47	0.09
				avg	0.08
				stdev	0.01

C.4.3.2. -C=O- errors in RPBE

The average error obtained for aldehydes and ketones is -0.21 eV, see Table C15.

TABLE C15

Calculated (RPBE) and experimental standard free energies in eV for aldehydes and ketones, and an assessment of their associated errors.

<i>Aldehydes/ketones</i>	ΔG_{DFT}°	ΔG_{EXP}°	ε_T	$\varepsilon_T - n_C \cdot \varepsilon_{CH_x}$
Formaldehyde	-1.27	-1.06	-0.21	-0.21
Acetaldehyde	-1.53	-1.38	-0.15	-0.23
Propanal	-1.35	-1.30	-0.06	-0.21
Butanal	-1.13	-1.18	0.05	-0.18
Acetone	-1.64	-1.58	-0.06	-0.22
			avg	-0.21
			stdev	0.02

C.4.3.3. $-(C=O)O-$ errors in RPBE

The average error for acids and esters is -0.27 eV. Thus, correcting this moiety by the CO_2 error (-0.46 eV) is not advisable.

TABLE C16

Calculated (RPBE) and experimental standard free energies in eV for carboxylic acids and esters in data set A, and an assessment of their associated errors.

<i>acids/esters</i>	ΔG_{DFT}°	ΔG_{EXP}°	ε_T	$\varepsilon_T - n_C \cdot \varepsilon_{CH_x}$
Formic Acid	-3.92	-3.64	-0.28	-0.28
Acetic Acid	-4.04	-3.88	-0.16	-0.24
Methyl formate	-3.34	-3.11	-0.23	-0.31
Methyl Acetate	-3.46	-3.39	-0.08	-0.23
			avg	-0.27
			stdev	0.04

C.4.3.4. $-OH$ errors in RPBE

To determine whether alcohols need a correction, we deconvoluted the total error from that of $-CH_x$. As the values in the column $\varepsilon_T - n_C \cdot \varepsilon_{CH_x}$ in Table C17 show that the isolated error is not substantial (-0.01 eV), we conclude that simple alcohols do not need corrections in RPBE, but methanol and ethanol might benefit from specific corrections in specialized studies.

TABLE C17

Calculated (RPBE) and experimental standard free energies in eV for alcohols in data set A, and an assessment of their associated errors.

<i>alcohol</i>	ΔG_{DFT}°	ΔG_{EXP}°	ε_T	$\varepsilon_T - n_C \cdot \varepsilon_{CH_x}$
Methanol	-1.67	-1.68	0.01	-0.07
Ethanol	-1.63	-1.74	0.11	-0.05
Propanol	-1.41	-1.68	0.27	0.04
Butanol	-1.22	-1.56	0.34	0.02
			avg	-0.01
			stdev	0.05

C.4.4. BEEF-vdW

C.4.4.1. -CH_x errors in BEEF-vdW

As shown in Table C18, -CH_x errors are large for this xc-functional compared to the others: 0.21 eV/CH_x.

TABLE C18

Calculated (BEEF-vdW) and experimental standard free energies in eV for the alkanes in data set A, and an assessment of their associated errors.

<i>-CH_x</i>		ΔG_{DFT}°	ΔG_{EXP}°	ε_T	ε_T/n_C
1	CH ₄	-0.27	-0.52	0.25	0.25
2	C ₂ H ₆	0.08	-0.33	0.41	0.21
3	C ₃ H ₈	0.34	-0.24	0.58	0.19
4	C ₄ H ₁₀	0.59	-0.19	0.78	0.20
5	C ₅ H ₁₂	0.85	-0.09	0.94	0.19
				avg	0.21
				stdev	0.03

C.4.4.2. -C=O- errors in BEEF-vdW

The errors in aldehydes and ketones are on average -0.27 eV, obtained after subtracting the contributions of -CH_x moieties.

TABLE C19

Calculated (BEEF-vdW) and experimental standard free energies in eV for aldehydes and ketones in data set A, and an assessment of their associated errors.

<i>aldehydes/ketones</i>	ΔG_{DFT}°	ΔG_{EXP}°	ε_T	$\varepsilon_T - n_C \cdot \varepsilon_{CH_x}$
Formaldehyd	-1.27	-1.06	-0.21	-0.21
e				
Acetaldehyde	-1.42	-1.38	-0.04	-0.25
Propanal	-1.18	-1.30	0.12	-0.30
Butanal	-0.88	-1.18	0.30	-0.33
Acetone	-1.45	-1.58	0.13	-0.28
			avg	-0.27
			stdev	0.04

C.4.4.3. $-(C=O)O-$ errors in BEEF-vdW

For BEEF-vdW this error is divided into 2 groups: that of carboxylic acids and that of esters (see Table 1). This is because the average calculated errors for the two groups differ by ~ 0.10 eV. In both cases the errors are different from that of CO_2 , see Tables S20-S21.

TABLE C20

Calculated (BEEF-vdW) and experimental standard free energies in eV for carboxylic acids in data set A, and an assessment of their associated errors.

<i>carboxylic acids</i>	ΔG_{DFT}°	ΔG_{EXP}°	ε_T	$\varepsilon_T - n_C \cdot \varepsilon_{CH_x}$
Formic Acid	-3.98	-3.64	-0.34	-0.34
Acetic Acid	-4.02	-3.88	-0.14	-0.34
			avg	-0.34
			stdev	0.00

TABLE C21

Calculated (BEEF-vdW) and experimental standard free energies in eV for esters in data set A, and an assessment of their associated errors.

<i>esters</i>	ΔG_{DFT}°	ΔG_{EXP}°	ϵ_T	$\epsilon_T - n_C \cdot \epsilon_{CH_x}$
Methyl formate	-3.36	-3.11	-0.25	-0.46
Metyl Acetate	-3.40	-3.39	-0.01	-0.43
			avg	-0.44
			stdev	0.02

C.4.4.4. -OH errors in BEEF-vdW

We find that the average error attributable to this functional group is -0.14 eV, see Table C22.

TABLE C22

Calculated (BEEF-vdW) and experimental standard free energies in eV for alcohols in data set A, and an assessment of their associated errors.

<i>alcohols</i>	ΔG_{DFT}°	ΔG_{EXP}°	ϵ_T	$\epsilon_T - n_C \cdot \epsilon_{CH_x}$
Methanol	-1.59	-1.68	0.09	-0.11
Ethanol	-1.47	-1.74	0.27	-0.14
Propanol	-1.18	-1.68	0.50	-0.12
Butanol	-0.93	-1.56	0.63	-0.20
			avg	-0.14
			stdev	0.04

C.4.4.5. H₂ errors in BEEF-vdW

The framework shown here assumes that H₂ is reasonably well described, so we do not provide an H₂ correction by default. However, we verified that correcting the H₂ formation energy by 0.085 eV together with the correction of the other errors also lowers the MAE of data set A. Such value agrees well with the reported value of 0.09 eV.^{8,9} Table C23 shows the corrections for the other types of errors when H₂ is corrected by 0.085 eV. We note that upon the H₂ correction, the values are rather similar to those of RPBE in Table 1.

TABLE C23

Gas-phase errors for BEEF-*vdW* with a simultaneous H₂ correction of 0.085 eV. The two values reported for $-(C=O)O-$ are for carboxylic acids and esters (the latter in parentheses).

<i>Error</i>	<i>BEEF-vdW</i>
CO ₂	-0.39
CO	-0.09
-C=O-	-0.21
-CH _x	0.08
-(C=O)O-	-0.24 (-0.30)
-OH	-0.08

Finally, we provide in Table C24 a compilation of data to show the progressive reduction in the errors as a result of the various corrections proposed in this study.

TABLE C24

Comparison of the initial mean absolute errors (MAE_{DFT}) for the CO₂ and CO reactions calculated with PBE, PW91, RPBE and BEEF-*vdW*, after applying corrections to the reactants ϵ_R (first correction, MAE_R), and after applying corrections to both the reactants ϵ_R and products ϵ_P (second correction, MAE_{RP}). $\%red_R = 100 \times (MAE_{DFT} - MAE_R) / MAE_{DFT}$, and $\%red_{RP} = 100 \times (MAE_{DFT} - MAE_{RP}) / MAE_{DFT}$.

<i>CO₂-based reactions</i>	<i>PBE</i>	<i>PW91</i>	<i>RPBE</i>	<i>BEEF-vdW</i>
MAE_{DFT} (eV)	0.43	0.30	1.14	1.53
MAE_R (eV)	0.10	0.09	0.18	0.31
MAE_{RP} (eV)	0.04	0.04	0.04	0.05
$\% red_R$	77%	68%	84%	80%
$\% red_{RP}$	91%	87%	96%	97%

<i>CO-based reactions</i>	<i>PBE</i>	<i>PW91</i>	<i>RPBE</i>	<i>BEEF-vdW</i>
MAE_{DFT} (eV)	0.61	0.68	0.27	0.65
MAE_R (eV)	0.10	0.09	0.19	0.32
MAE_{RP} (eV)	0.04	0.04	0.04	0.05
$\% red_R$	84%	87%	29%	50%
$\% red_{RP}$	94%	95%	85%	92%

C.5 Electrocatalysis-related data

Figures C5 and C6 compare CO_2 RR to CO on Au(100) and Au(110) single-crystal electrodes using PBE with (panel b) and without (panel a) gas-phase corrections applied to CO_2 and CO.

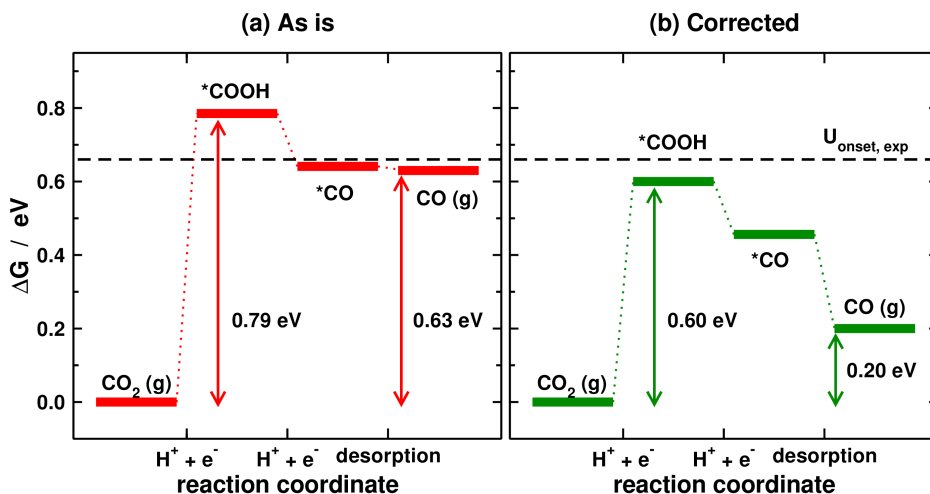
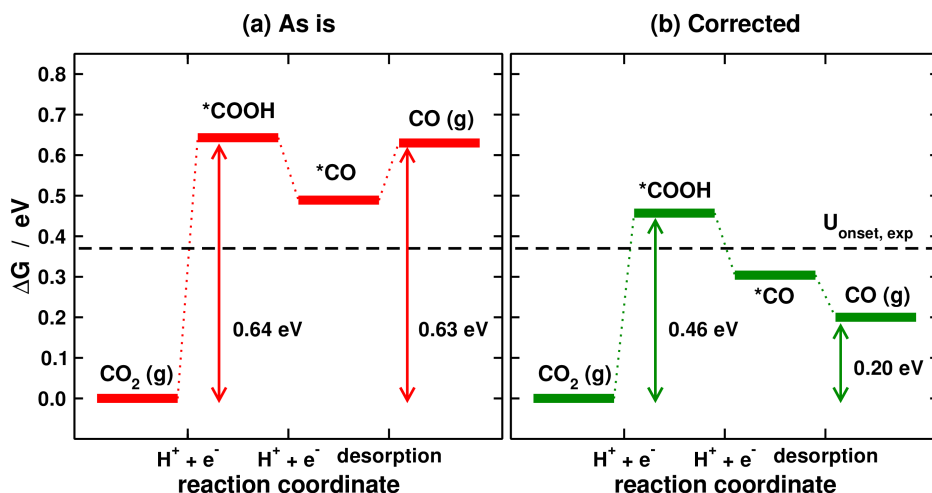


FIGURE C5

Free energy diagrams for CO_2 reduction to CO using Au(100) single-crystal electrodes. (a) Using DFT data as is, and (b) correcting CO_2 and CO for their gas-phase errors. The black dashed line at 0.66 eV marks the free energy corresponding to the experimental onset potential of -0.66 V vs RHE.¹⁰

Table C25 contains the experimental and computational data included in Figures 4.3 and 4.4 in the main text. Cu_{poly} and Ag_{poly} are simulated by missing-row reconstructed Cu(110) and Ag(110). Au_{poly} is represented by Au(211). For each electrode in Table C25 the corresponding slabs contained four layers: the bottommost two were fixed at the optimized bulk positions and the uppermost two and the adsorbates were completely free to relax.

**FIGURE C6**

Free energy diagrams for CO₂ reduction to CO using Au(110) single-crystal electrodes. (a) Using DFT data as is, and (b) correcting CO₂ and CO for their gas-phase errors. The black dashed line at 0.37 eV marks the free energy corresponding to the experimental onset potential of -0.37 V vs RHE.¹⁰

TABLE C25

Experimental, DFT calculated and semiempirically corrected onset potentials (in V vs RHE) for CO₂ electroreduction to CO on various metal electrodes.

Electrode	U_{DFT}	$U_{corrected}$	U_{exp}
Au(111)	-0.90	-0.71	-0.66 (ref. ¹⁰)
Au(110)	-0.64	-0.46	-0.37 (ref. ¹⁰)
Au(100)	-0.87	¹⁸ -0.69	-0.66 (ref. ¹⁰)
Au _{poly}	-0.53	-0.34	-0.26 (ref. ¹¹)
Ag(111)	-1.09	-0.90	-0.94 (ref. ¹²)
Ag _{poly}	-0.83	-0.65	-0.60 (ref. ¹³)
Cu _{poly}	-0.53	-0.34	-0.40 (ref. ¹¹)

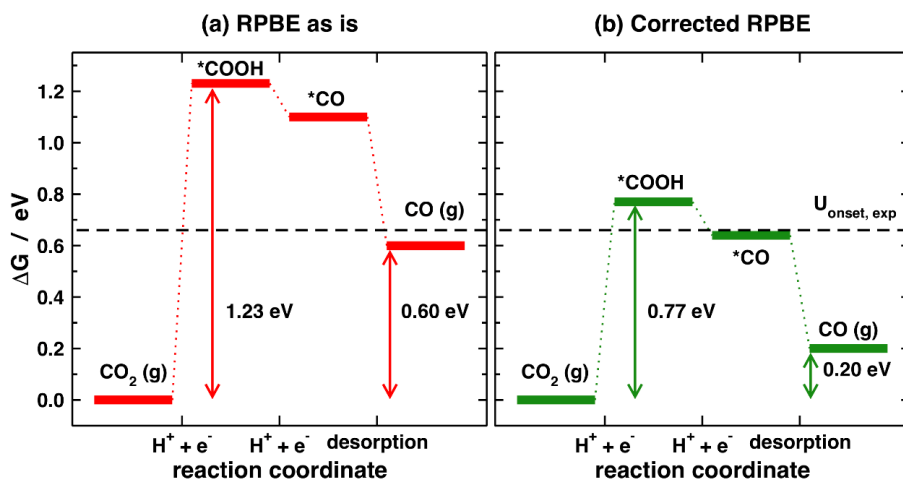
The ZPE, vibrational entropy and solvation corrections of *COOH and *CO can be found in Table C26. The solvation corrections were assessed from calculations in which water molecules were present/absent in the proximities¹⁴ of the adsorbates and are in line with previous reports.^{15,16}

TABLE C26

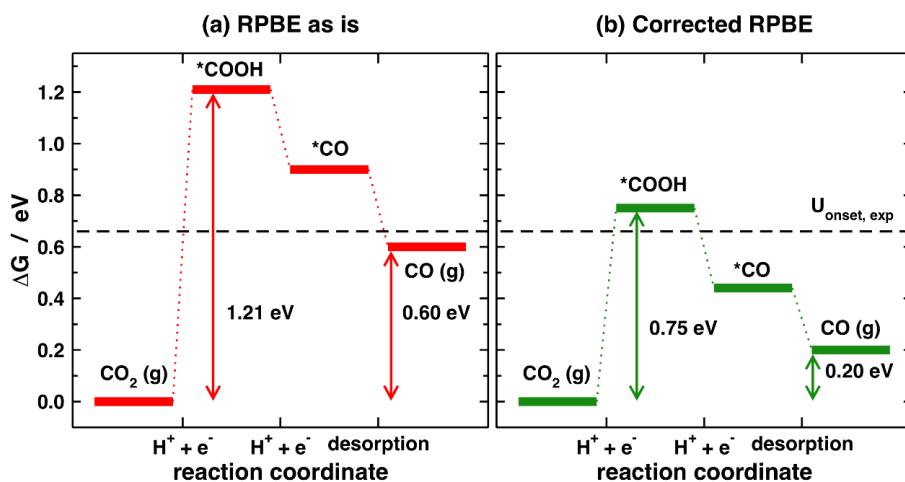
Zero-point, entropic and solvation contributions (in eV) to the free energies of *COOH and *CO on various metal electrodes.

<i>Electrode</i>	<i>ZPE</i>	<i>TS_{vib}</i>	<i>E_{solvation}</i>
<i>COOH @ Au(111)</i>	0.60	0.34	-0.42
<i>CO @ Au(111)</i>	0.17	0.15	0.00
<i>COOH @ Au(110)</i>	0.60	0.34	-0.42
<i>CO @ Au(110)</i>	0.17	0.15	0.00
<i>COOH @ Au(100)</i>	0.61	0.29	-0.42
<i>CO @ Au(100)</i>	0.19	0.16	0.00
<i>COOH @ Au_{poly}</i>	0.60	0.34	-0.42
<i>CO @ Au_{poly}</i>	0.17	0.15	0.00
<i>COOH @ Ag(111)</i>	0.59	0.26	-0.44
<i>CO @ Ag(111)</i>	0.16	0.25	0.00
<i>COOH @ Ag_{poly}</i>	0.59	0.28	-0.44
<i>CO @ Ag_{poly}</i>	0.16	0.25	0.00
<i>COOH @ Cu_{poly}</i>	0.62	0.22	-0.28
<i>CO @ Cu_{poly}</i>	0.16	0.14	0.00

Finally, we modelled CO₂ electroreduction to CO on Au(111) and Au(100) with RPBE. The equilibrium potential is -0.30 V vs RHE before the corrections and -0.10 V vs RHE after the corrections (it is -0.10 V vs RHE in experiments). The ZPE, vibrational entropy and solvation corrections of *COOH (0.61, 0.29 eV) and *CO (0.17, 0.16 eV) are similar to those of PBE (see Table C26), and the solvation corrections are assumed to be the same. We compare in Figures C7-C8 the calculated onset potentials with the experimental ones in reference¹⁰, namely -0.66 V vs RHE for both facets. Without corrections, the onset potentials on Au(111) and Au(100) are -1.23 and -1.21 V vs RHE, giving errors of 0.57 and 0.55 V. Upon the corrections, the onset potentials are -0.77 and -0.75 V, giving errors of 0.11 and 0.09 V.

**FIGURE C7**

Free energy diagrams for CO₂ reduction to CO using Au(111) single-crystal electrodes. (a) Using DFT-RPBE data as is, and (b) correcting CO₂ and CO for their gas-phase errors. The black dashed line at 0.66 eV marks the free energy corresponding to the experimental onset potential of -0.66 V vs RHE.¹⁰

**FIGURE C8**

Free energy diagrams for CO₂ reduction to CO using Au(100) single-crystal electrodes. (a) Using DFT-RPBE data as is, and (b) correcting CO₂ and CO for their gas-phase errors. The black dashed line at 0.66 eV marks the free energy corresponding to the experimental onset potential of -0.66 V vs RHE.¹⁰

C.6 Interlayer cohesive energy in graphite

Table C27 contains a literature survey on the experimental interlayer cohesive and/or binding energy of graphite, see Table R1. The values are in the range of 0.031 – 0.064 eV/atom,^{17–22} and the average value is 0.046 eV/atom. This reflects the common notion that graphite layers are linked via weak van der Waals interactions and justifies the approximation of graphite by graphene for our current purposes.

TABLE C27

Experimental interlayer energy of interaction for graphite described by interlayer cohesive energies (CE) and interlayer binding energies (BE).

<i>Energy (eV/atom)</i>	<i>Interlayer interaction</i>	<i>Source</i>
0.064	CE	[17]
0.054	BE	[17]
0.043	CE	[18]
0.052	CE	[19]
0.035	CE	[20]
0.031	BE	[20]
0.055	BE	[21]
0.031	BE	[22]

C.7 Alternative analysis using training and extrapolation sets

We have also split the molecules in Data set A into a training set of 21 molecules and an extrapolation set of seven molecules (pentane, butanal, glyoxal, isopropanol, butanol, and methyl acetate) and added a new molecule (butanone). Note that the extrapolation set is formed by the largest molecules in every family of compounds (which helps in assessing the performance of the method as the molecules' size increases). The new errors were pinpointed in the training set exactly as described in section 4, Tables C6-C22. Table C28 shows that the errors are similar in the training set compared to the full set, being the average difference of only 0.01 eV. In general, we have observed that only one or two compounds are necessary to pinpoint a specific error, so the training set may easily be made smaller without compromising the accuracy of the method.

TABLE C28

Comparison of the gas-phase corrections determined with the entire Data set A (in grey), and with a training set of 21 molecules (in white). All values are in eV.

Error	PBE		PW91		RPBE		BEEF-vdW	
-CHx	0.02	0.03	-0.01	-0.01	0.07	0.08	0.21	0.21
-C=O-	-0.11	-0.10	-0.11	-0.10	-0.22	-0.21	-0.27	-0.27
-(C=O)O-	-0.20	-0.19	-0.19	-0.19	-0.27	-0.27	-0.34 (-0.44)	-0.34 (-0.47)
-OH	-0.05	-0.04	-0.04	-0.04	-0.03	-0.01	-0.14	-0.14

Moreover, we extrapolated the corrections obtained in the training set to the extrapolation set for the formation energies, and the CO₂ reduction and CO reduction energies. Tables C29-C31 show the free energies for the four functionals under study, the corrected free energies and the experimental values, providing in all cases the mean absolute errors (MAEs) with respect to experiments. From Tables C29-C31 we conclude that the MAEs are significantly decreased in the extrapolation set for the formation energies and those involved in CO₂ and CO reduction reactions. Importantly, the final MAEs are comparable to those in Figures 4.1-4.2. Since the MAEs for a given functional are identical for the three corrected energies (see the bottom rows for the corrected functionals in Tables C29-C31), the errors do not appear to propagate in our method. Conversely, the errors grow rapidly among the uncorrected energies, particularly for RPBE and BEEF-vdW.

TABLE C29

Formation energies of the compounds in the extrapolation set. All values are in eV.

<i>Species</i>	ΔG_{PBE}	ΔG_{PW91}	ΔG_{RPBE}	$\Delta G_{BEEF-vdW}$	ΔG_{PBE}^{corr}	ΔG_{PW91}^{corr}	ΔG_{RPBE}^{corr}	$\Delta G_{BEEF-vdW}^{corr}$	ΔG_{exp}
<i>pentane</i>	0.09	-0.06	0.38	0.85	-0.04	-0.02	0.01	-0.21	-0.09
<i>butanal</i>	-1.19	-1.27	-1.13	-0.88	-1.15	-1.14	-1.14	-1.25	-1.18
<i>butanone</i>	-1.54	-1.63	-1.45	-1.20	-1.51	-1.50	-1.46	-1.57	-1.52
<i>glyoxal</i>	-2.13	-2.14	-2.39	-2.46	-1.92	-1.93	-1.96	-1.92	-1.97
<i>isopropanol</i>	-1.73	-1.81	-1.52	-1.30	-1.76	-1.75	-1.71	-1.79	-1.80
<i>butanol</i>	-1.48	-1.58	-1.22	-0.93	-1.53	-1.51	-1.49	-1.64	-1.56
<i>methyl acetate</i>	-3.51	-3.56	-3.46	-3.40	-3.37	-3.35	-3.34	-3.38	-3.39
<i>MAE</i>	0.09	0.09	0.24	0.46	0.03	0.04	0.06	0.05	

TABLE C30Free energies for CO₂ reduction to the compounds in the extrapolation set. All values are in eV.

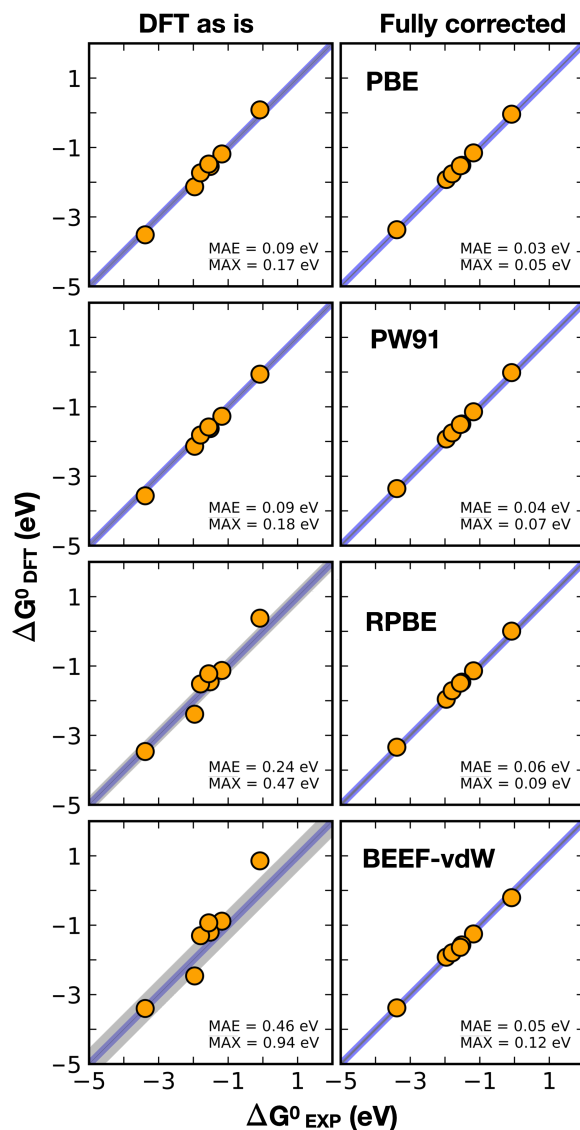
<i>Species</i>	ΔG_{PBE}	ΔG_{PW91}	ΔG_{RPBE}	$\Delta G_{BEEF-vdW}$	ΔG_{PBE}^{corr}	ΔG_{PW91}^{corr}	ΔG_{RPBE}^{corr}	$\Delta G_{BEEF-vdW}^{corr}$	ΔG_{exp}
<i>pentane</i>	-2.24	-2.58	-0.56	0.40	-3.29	-3.27	-3.25	-3.46	-3.34
<i>butanal</i>	-0.67	-0.92	0.49	1.12	-1.39	-1.38	-1.37	-1.49	-1.42
<i>butanone</i>	-1.03	-1.28	0.16	0.80	-1.75	-1.73	-1.70	-1.80	-1.75
<i>glyoxal</i>	1.68	1.59	1.97	2.10	1.52	1.51	1.48	1.52	1.47
<i>isopropanol</i>	-0.75	-0.96	0.29	0.80	-1.34	-1.33	-1.29	-1.38	-1.38
<i>butanol</i>	-0.96	-1.23	0.39	1.07	-1.76	-1.74	-1.73	-1.87	-1.79
<i>methyl acetate</i>	-0.17	-0.34	0.71	1.07	-0.58	-0.57	-0.55	-0.59	-0.60
<i>MAE</i>	0.67	0.44	1.75	2.31	0.03	0.04	0.06	0.05	-

TABLE C31

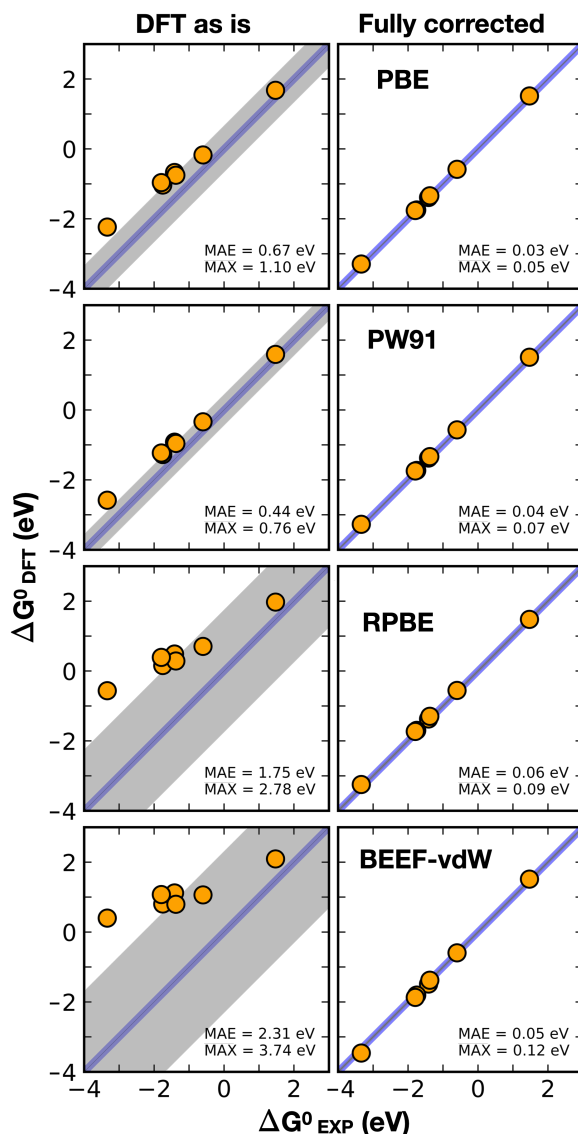
Free energies for CO reduction to the compounds in the extrapolation set. All values are in eV.

<i>Species</i>	ΔG_{PBE}	ΔG_{PW91}	ΔG_{RPBE}	$\Delta G_{BEEF-vdW}$	ΔG_{PBE}^{corr}	ΔG_{PW91}^{corr}	ΔG_{RPBE}^{corr}	$\Delta G_{BEEF-vdW}^{corr}$	ΔG_{exp}
<i>pentane</i>	-5.87	-6.05	-3.98	-2.99	-4.77	-4.75	-4.73	-4.94	-4.82
<i>butanal</i>	-3.58	-3.69	-2.25	-1.59	-2.57	-2.56	-2.56	-2.67	-2.60
<i>butanone</i>	-3.94	-4.05	-2.58	-1.91	-2.93	-2.92	-2.88	-2.99	-2.94
<i>glyoxal</i>	0.23	0.21	0.60	0.74	0.93	0.92	0.89	0.92	0.88
<i>isopropanol</i>	-2.93	-3.03	-1.77	-1.24	-2.23	-2.22	-2.18	-2.27	-2.27
<i>butanol</i>	-3.87	-4.00	-2.34	-1.64	-2.95	-2.93	-2.91	-3.06	-2.98
<i>methyl acetate</i>	-2.35	-2.42	-1.34	-0.97	-1.47	-1.46	-1.44	-1.48	-1.49
<i>MAE</i>	0.87	0.97	0.44	0.99	0.03	0.04	0.06	0.05	-

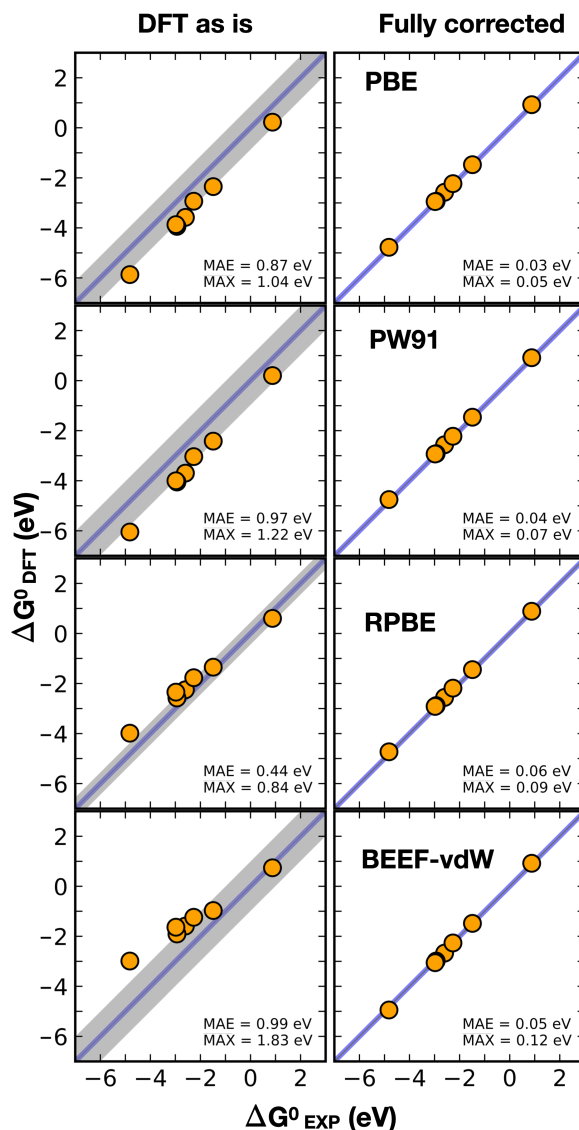
With the values in Tables C29-C31 we prepared Figures C9-C11. The figures display the data as parity plots comparing experimental and computational data without any corrections and applying all the corrections listed in Table C28. The plots illustrate that: (i) the errors are considerably decreased upon applying the corrections, (ii) the errors do not propagate in our method, (iii) the errors propagate quickly in as-is DFT as the molecules become larger (i.e. as ΔG gets increasingly negative in Figures C10-C11).

**FIGURE C9**

Parity plots for the experimental and DFT-calculated free energies of formation of the molecules in the extrapolation set using PBE, PW91, RPBE and BEEF-vdW. The left column shows the data calculated with DFT without any correction, the right column shows the data after correcting for all the errors detected in the training set. The mean and maximum absolute errors (MAE, MAX) are shown in each case. The grey area is \pm MAE in each case. The blue shaded area around the parity line covers an area of ± 0.15 eV.

**FIGURE C10**

Parity plots for the experimental and DFT-calculated free energies for the production of the molecules in the extrapolation set from CO_2 and H_2 using PBE, PW91, RPBE and BEEF-vdW. The left column shows the data calculated with DFT without any correction. The right column shows the data after correcting for errors in CO_2 and the products. The mean and maximum absolute errors (MAE, MAX) are shown in each case. The grey area is \pm MAE in each case. The blue shaded area around the parity line covers an area of ± 0.15 eV.

**FIGURE C11**

Parity plots for the experimental and DFT-calculated free energies for the production of the molecules in the extrapolation set from CO and H₂ using PBE, PW91, RPBE and BEEF-vdW. The left column shows the data calculated with DFT without any correction. The right column shows the data after correcting for errors in CO and the products. The mean and maximum absolute errors (MAE, MAX) are shown in each case. The grey area is \pm MAE in each case. The blue shaded area around the parity line covers an area of \pm 0.15 eV.

C.8 References

- (1) Kurth, S.; Perdew, J. P.; Blaha, P. Molecular and Solid-State Tests of Density Functional Approximations: LSD, GGAs, and Meta-GGAs. *Int. J. Quantum Chem.* 1999, 75, 889-909.
- (2) Calle-Vallejo, F.; Martínez, J. I.; García-Lastra, J. M.; Mogensen, M.; Rossmeisl, J. Trends in Stability of Perovskite Oxides. *Angew. Chem. Int. Ed.* 2010, 49, 7699-7701.
- (3) Martínez, J. I.; Hansen, H. A.; Rossmeisl, J.; Nørskov, J. K. Formation Energies of Rutile Metal Dioxides Using Density Functional Theory. *Phys. Rev. B* 2009, 79, 045120.
- (4) Bartel, C. J.; Weimer, A. W.; Lany, S.; Musgrave, C. B.; Holder, A. M. The Role of Decomposition Reactions in Assessing First-Principles Predictions of Solid Stability. *Npj Comput. Mater.* 2019, 5, 1-9.
- (5) Lide, D. R. *CRC Handbook of Chemistry and Physics*, 85th Edition; CRC Press, 2004.
- (6) M. W. Chase; C. A. Davies; J. R. Downey; D. J. Frurip; R. A. MacDonald; A. N. Syverud. NIST-JANAF Thermochemical Tables. *J. Phys. Chem. Ref. Data* 1985, Suppl. 1 to Vol. 14, 1856.
- (7) Informatics, N. O. of D. and. NIST Chemistry WebBook <https://webbook.nist.gov/chemistry/> (accessed Oct 18, 2019).
- (8) Studt, F.; Behrens, M.; Kunkes, E. L.; Thomas, N.; Zander, S.; Tarasov, A.; Schumann, J.; Frei, E.; Varley, J. B.; Abild-Pedersen, F.; Nørskov, J. K.; Schlögl, R. The Mechanism of CO and CO₂ Hydrogenation to Methanol over Cu-Based Catalysts. *ChemCatChem* 2015, 7, 1105-1111.
- (9) Studt, F.; Abild-Pedersen, F.; Varley, J. B.; Nørskov, J. K. CO and CO₂ Hydrogenation to Methanol Calculated Using the BEEF-VdW Functional. *Catal. Lett.* 2013, 143, 71-73.
- (10) Todoroki, N.; Tei, H.; Tsurumaki, H.; Miyakawa, T.; Inoue, T.; Wadayama, T. Surface Atomic Arrangement Dependence of Electrochemical CO₂ Reduction on Gold: Online Electrochemical Mass Spectrometric Study on Low-Index Au(Hkl) Surfaces. *ACS Catal.* 2019, 9, 1383-1388.
- (11) Kuhl, K. P.; Hatsukade, T.; Cave, E. R.; Abram, D. N.; Kibsgaard, J.; Jaramillo, T. F. Electrocatalytic Conversion of Carbon Dioxide to Methane and Methanol on Transition Metal Surfaces. *J. Am. Chem. Soc.* 2014, 136, 14107-14113.
- (12) Hoshi, N.; Kato, M.; Hori, Y. Electrochemical Reduction of CO₂ on Single Crystal Electrodes of Silver Ag(111), Ag(100) and Ag(110). *J. Electroanal. Chem.* 1997, 440, 283-286.
- (13) Ma, M.; Trzeźniewski, B. J.; Xie, J.; Smith, W. A. Selective and Efficient Reduction of Carbon Dioxide to Carbon Monoxide on Oxide-Derived Nanostructured Silver Electrocatalysts. *Angew. Chem. Int. Ed.* 2016, 55, 9748-9752.
- (14) Calle-Vallejo, F.; F. de Morais, R.; Illas, F.; Loffreda, D.; Sautet, P. Affordable Estimation of Solvation Contributions to the Adsorption Energies of Oxygenates on Metal Nanoparticles. *J. Phys. Chem. C* 2019, 123, 5578-5582.

- (15) Peterson, A. A.; Abild-Pedersen, F.; Studt, F.; Rossmeisl, J.; Nørskov, J. K. How Copper Catalyzes the Electroreduction of Carbon Dioxide into Hydrocarbon Fuels. *Energy Environ. Sci.* 2010, 3, 1311-1315.
- (16) Calle-Vallejo, F.; Koper, M. T. M. Theoretical Considerations on the Electroreduction of CO to C2 Species on Cu(100) Electrodes. *Angew. Chem. Int. Ed.* 2013, 52, 7282-7285.
- (17) Wang, W.; Dai, S.; Li, X.; Yang, J.; Srolovitz, D. J.; Zheng, Q. Measurement of the Cleavage Energy of Graphite. *Nat. Commun.* 2015, 6, 1-7.
- (18) Girifalco, L. A.; Lad, R. A. Energy of Cohesion, Compressibility, and the Potential Energy Functions of the Graphite System. *J. Chem. Phys.* 1956, 25, 693-697.
- (19) Zacharia, R.; Ulbricht, H.; Hertel, T. Interlayer Cohesive Energy of Graphite from Thermal Desorption of Polyaromatic Hydrocarbons. *Phys. Rev. B* 2004, 69, 155406.
- (20) Benedict, L. X.; Chopra, N. G.; Cohen, M. L.; Zettl, A.; Louie, S. G.; Crespi, V. H. Microscopic Determination of the Interlayer Binding Energy in Graphite. *Chem. Phys. Lett.* 1998, 286, 490-496.
- (21) Xia, M.; Liang, C.; Cheng, Z.; Hu, R.; Liu, S. The Adhesion Energy Measured by a Stress Accumulation-Peeling Mechanism in the Exfoliation of Graphite. *Phys. Chem. Chem. Phys.* 2019, 21, 1217-1223.
- (22) Liu, Z.; Liu, J. Z.; Cheng, Y.; Li, Z.; Wang, L.; Zheng, Q. Interlayer Binding Energy of Graphite: A Mesoscopic Determination from Deformation. *Phys. Rev. B* 2012, 85, 205418.

D: Supporting Information for Chapter 5

D1 Experimental

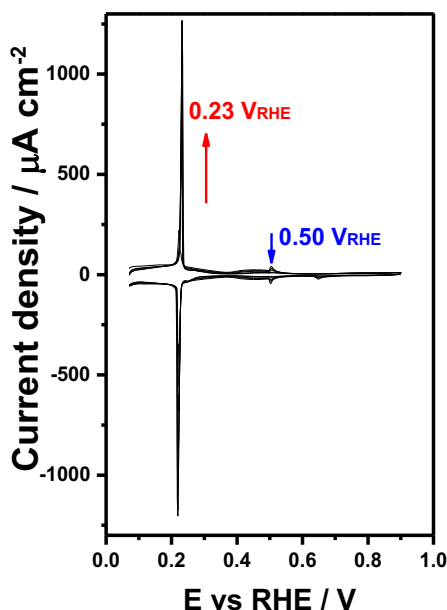
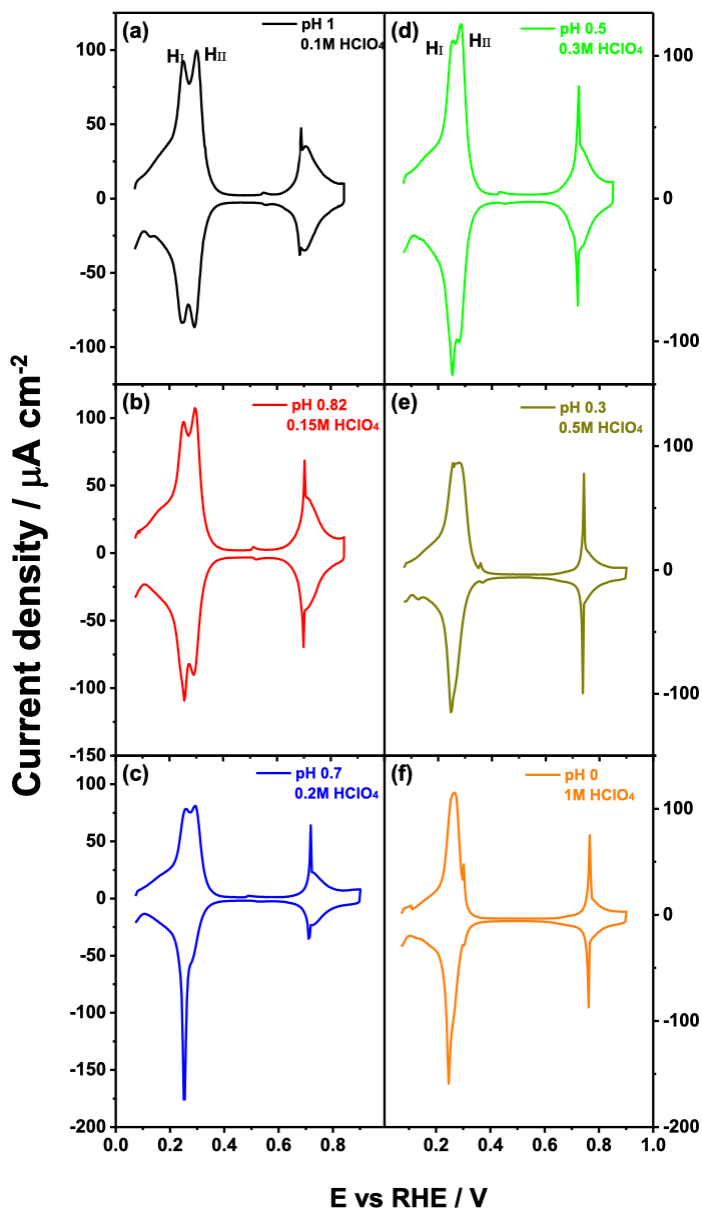


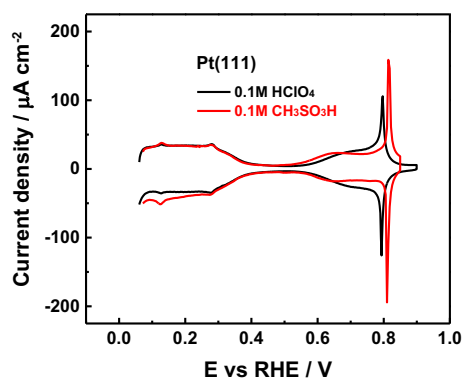
FIGURE D1

Electrochemical deposition of a palladium monolayer on Pt(111) electrode from 0.1 M H_2SO_4 + 0.1 mM PdSO_4 . Scan rate: 50 mV s^{-1} . Arrows indicate the evolution with time.

Figure D1 shows the effect of the progressive accumulation of palladium on the Pt(111) electrode surface on the voltammetric profile of the electrode during the electrochemical deposition of a palladium monolayer. Initially, the presence of palladium on the surface is reflected by the growth of a sharp adsorption state at 0.23 V_{RHE} , concomitant with the progressive decrease of the characteristic adsorption states of Pt(111) in 0.1 M H_2SO_4 . In addition, the presence of the characteristic spike of Pt(111) at 0.50 V_{RHE} strongly suggests the existence of wide Pt(111) domains. With increasing deposition cycles the last contributions from the Pt(111) domains around 0.50 V_{RHE} disappear. Previous studies using scanning tunnelling microscopy (STM) showed that a complete pseudomorphic monolayer of Pd is formed prior to bulk deposition during electrochemical deposition of Pd on Pt(111).¹ The voltammetric charge of (bi)sulfate adsorption at 0.23 V_{RHE} can be related in a quantitative way to the palladium coverage and corresponds to a charge of 320 $\mu\text{C cm}^{-2}$ for $\text{Pd}_{\text{ML}}\text{Pt}(111)$.²

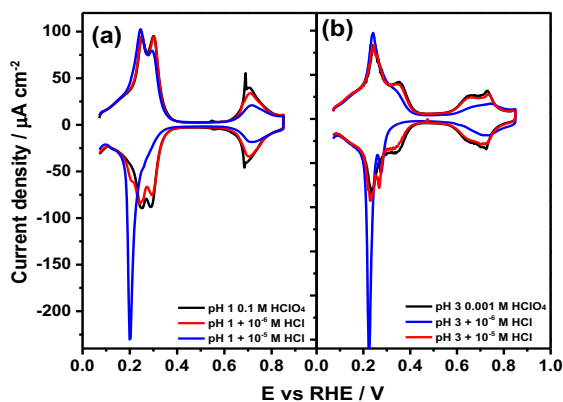
**FIGURE D2**

Cyclic voltammogram of $\text{Pd}_{\text{ML}}\text{Pt}(111)$ electrode recorded in (a) 0.1 M HClO_4 (pH = 1), (b) 0.15 M HClO_4 (pH = 0.82), (c) 0.2 M HClO_4 (pH = 0.7), (d) 0.3 M HClO_4 (pH = 0.5), (e) 0.5 M HClO_4 (pH = 0.3) and (f) 1 M HClO_4 (pH = 0). Scan rate: 50 mV s^{-1} .

**FIGURE D3**

Cyclic voltammogram of Pt(111) in 0.1 M HClO₄ and 0.1 M CH₃SO₃H. Scan rate: 50 mV s⁻¹.

Figure D3 compares the cyclic voltammograms of a Pt(111) electrode recorded in 0.1 M HClO₄ and 0.1 M CH₃SO₃H. At potentials lower than 0.55 V_{RHE}, where the hydrogen adsorption/desorption and the double-layer regions take place, there is an almost perfect coincidence between the curves. However, at higher potentials, when the adsorption of oxygen-containing species occurs, visible differences between the CVs appear. At potentials in the range of 0.55 to 0.90 V_{RHE}, where adsorption of hydroxyl from water dissociation is expected, OH adsorption starts at slightly lower potentials in CH₃SO₃H than in HClO₄ and this could suggest weak specific adsorption. In contrast, the following sharp peak, the spike of the so-called "butterfly" feature, is slightly shifted to higher potentials in 0.1 M CH₃SO₃H.

**FIGURE D4**

Cyclic voltammogram of Pd_{ML}Pt(111) electrode recorded in (a) 0.1 M HClO₄ (pH = 1) and (b) 0.001 M HClO₄ (pH = 3), without and with different concentrations of Cl⁻. Scan rate: 50 mV s⁻¹.

Figure D4 shows the cyclic voltammograms of the Pd_{ML}Pt(111) electrode recorded in (a) 0.1 M HClO₄ (pH = 1) and (b) 0.001 M HClO₄ (pH = 3) with small concentrations (10⁻⁶ and 10⁻⁵ M) of Cl⁻. The change caused by Cl⁻ is the same as reported by Markovic et al³: the observed H_I and H_{II} peaks exhibit asymmetry, in contrast to the symmetric peaks observed in solutions containing only HClO₄. Therefore, chloride is in competition with H_{upd} as well as with OH_{ads}.

D2 Computational methods

All of the calculations were performed using the Vienna Ab initio Simulation Package (VASP)⁴ with the Generalized-Gradient-Approximation (GGA) PBE exchange-correlation functional⁵ and the projector-augmented wave (PAW) method.⁶ The plane-wave energy cut-off was 450 eV. Pt(111) and Pd_{ML}Pt(111) surfaces were modeled using a slab consisting of a (3×3) unit cell. After verifying energy convergence with respect to atomic layers we decided to use 6 atomic layers for Pd_{ML}Pt(111) and Pt(111), in this way providing a convergence criterion of adsorption energies to ≤ 0.05 eV. The k-point sampling grids used for both surfaces were (6×6×1) generated using the Monkhorst-Pack approach.^{[4-6][4-6]7}

To account for bulk effects in a finite slab, the first two atomic layers were kept fixed at the PBE optimized lattice constant of Pt (3.98 Å) while the remaining atomic layers were relaxed. We included empirical van der Waals (vdW) corrections through the DFT-D3(BJ)^{8,9} method on PBE, here denoted as PBED3, to the calculations for a comparison of the energetics of the water-water and water-metal interactions. The relaxations to find the ground-state configurations were made using the quasi-Newton algorithm. Site analysis and geometry optimizations were performed until the forces were smaller than 0.02 eV Å⁻¹. To prevent spurious interactions between the slabs along the z axis, a vacuum of ~15.0 Å was set for all cases and dipole corrections were also applied by adding the tags LDIPOL=.TRUE. and IDIPOL = 3. The slab was positioned at the bottom of the cell, in this way assuring convergence when using the dipole moment corrections. Several attempts with the cell positioned in the center plus dipole corrections failed to converge.

For the surfaces and adsorbed species, the method of Methfessel-Paxton¹⁰ to the second order was used to set the partial occupancies on each orbital and the smearing width was set to 0.2 eV. For the individual molecules, a Gaussian smearing with a width of 0.001 eV was used instead. The gas-phase molecules, H₂O(g), H₂(g), ClO₂(g), F₂(g) and SO₂(g) were simulated in an asymmetric box of (15.0×15.1×15.3) Å³ at the gamma point (1×1×1).

D3 Gibbs Free Energy of Adsorption

The changes in free energies of adsorption were calculated using the hypothetical chemical reaction 1, following Eq. D.2. A(g) is a gas-phase molecule, * is the surface and *A is the adsorbed species on the surface.



$$\Delta G_{ads}^{*A} = G^{*A} - G_{(g)}^A - G^* \quad \text{D.2}$$

Where,

$$G^{*A} = E_{DFT}^{*A} + ZPE^{*A} - TS_{vib}^{*A} \quad \text{D.3}$$

$$G_{(g)}^A = E_{DFT(g)}^A + ZPE_{(g)}^A - TS_{trans, rot, vib(g)}^A \quad \text{D.4}$$

$$G^* = E_{DFT}^* \quad \text{D.5}$$

where E_{DFT}^x is the relative energy from the optimization extrapolated to 0 K ($\sigma \rightarrow 0$) where x refers to either *A, A(g) or (*), ZPE is the zero-point energy and TS is the entropy contribution at 298.15 K. For the gas-phase molecules, the entropy includes all contributions, and was obtained from standard thermodynamic tables.¹¹ For the adsorbed species, the entropy includes only the vibrational contributions and was calculated using statistical mechanics equations within the harmonic oscillator approximation.¹² These contributions were obtained by performing a vibrational analysis within the VASP code using several displacements around the ground state. Within this method only the adsorbed species are displaced in all directions while the slab is kept fixed.

To obtain the solution-phase free energy of water from DFT-calculated gas-phase water, we corrected the energy by adding -0.087 eV to the TS term.¹³ This represents the difference between the free energy of formation of gas-phase water and liquid-phase water at 298.15 K.

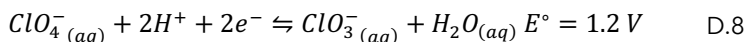
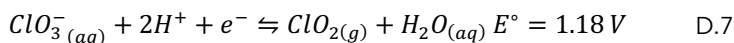
The potential dependence of all the proton-coupled electron transfer reactions was calculated using the computational hydrogen electrode (CHE) model,¹³ where at equilibrium and standard conditions (0 V and a pressure of 1 atm), the protons in solution and the electrons in the electrode ($H^+(aq)$, e^-) are in equilibrium with $H_2(g)$, as shown in the following chemical equation:



With this thermodynamic convention we can overcome the computational difficulty of calculating the energy of protons and electrons in DFT and instead calculate the ground-state free energy of a $H_2(g)$ molecule. Half of that energy will then represent the free energy of the coupled proton and electron as shown in Eq D.6.^{13,14}

The solution-phase free energies of perchlorate, sulfate and bisulfate anions were calculated via a thermodynamic cycle combining DFT free energies and tabulated experimental standard redox chemical potentials at standard conditions (298.15 K and 1 atm), as a direct calculation of these anion free energies would be difficult with DFT due to the long length and time scales of the solvation energetics. Using an electrochemical thermodynamic cycle allows us to calculate the solution-phase free energy of an anion from a neutral, typically gas-phase, species, such that its energy can be accurately determined with DFT as $G = \text{ZPE} - \text{TS} + \text{PV}$. This is analogous to the computational hydrogen electrode method, except it requires experimentally measured equilibrium potentials, whereas in the computational hydrogen electrode method, the equilibrium potential between hydrogen gas and aqueous protons at standard conditions is defined to be exactly 0 V, i.e., $G_{e^-} = -n |e| U^\circ = 0$

As an example, the solution-phase free energy of ClO_4^- is discussed below. Using the following redox equations at standard conditions, we can use the calculated free energy of ClO_2 to calculate the free energy of aqueous perchlorate.



From Eq. D.7, ClO_3^- free energy can be determined which can then be used in Eq. D.8 to determine the solution-phase free energy of ClO_4^- . Note that the free energy of the electron is, $G_{e^-} = -n |e| U^\circ$ and the total free energy is, $\Delta G = \Delta G^\circ - k_b \ln(10) \text{pH}$, where the second term of the equation is 0 at $\text{pH} = 0$ and at equilibrium $\Delta G = 0$. Therefore, the free energy of Eq. D.7 is

$$\Delta G = G_{(g)}^{\text{ClO}_2} + G_{(aq)}^{\text{H}_2\text{O}} - G_{(aq)}^{\text{ClO}_3^-} - G_{(g)}^{\text{H}_2} - G_{e^-} \quad \text{D.9}$$

Substituting $G_{e^-} = -n |e| U^\circ$, and $E^\circ = U^\circ$:

$$G_{(aq)}^{\text{ClO}_3^-} = G_{(g)}^{\text{ClO}_2} + G_{(aq)}^{\text{H}_2\text{O}} - G_{(g)}^{\text{H}_2} - (-n |e| U^\circ) \quad \text{D.10}$$

$$G_{(aq)}^{\text{ClO}_3^-} = G_{(g)}^{\text{ClO}_2} + G_{(aq)}^{\text{H}_2\text{O}} - G_{(g)}^{\text{H}_2} + 1.18 \text{ eV} \quad \text{D.11}$$

Similarly,

$$G_{(aq)}^{\text{ClO}_4^-} = G_{(aq)}^{\text{ClO}_3^-} + G_{(aq)}^{\text{H}_2\text{O}} - G_{(g)}^{\text{H}_2} + 2.4 \text{ eV} \quad \text{D.12}$$

Now, the calculated free energy of the proton in solution is obtained following the definition that the standard hydrogen electron redox potential is set to 0 V on the SHE scale.

Given the previous definitions:

$$\frac{1}{2}H_{2(g)} \rightleftharpoons H^+_{aq} + e^- \quad E^\circ = 0V \quad D.13$$

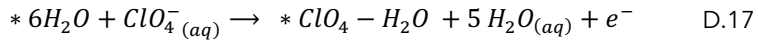
$$\Delta G = G_{(aq)}^{H^+} - n|e|U - \frac{1}{2}G_{(g)}^{H_2} \quad D.14$$

Then,

$$0 = G_{(aq)}^{H^+} - 1x e(0V) - \frac{1}{2}G_{(g)}^{H_2} \quad D.15$$

$$\frac{1}{2}G_{(g)}^{H_2} = G_{(aq)}^{H^+} \quad D.16$$

Then, the adsorption energy of perchlorate on the surface is calculated as follows: Given the following reaction, where we used an adsorbed water adlayer as the reference state $^*6 H_2O$ then,



represents the adsorbed perchlorate co-adsorbed with one water molecule. Then, we can determine the change in free energy of adsorption of adsorbed solvated perchlorate as shown below in Eq. D18.

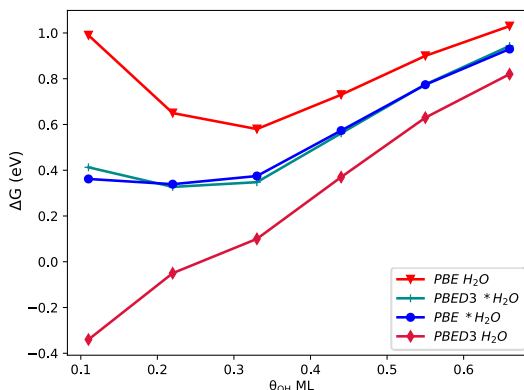
$$\Delta G_{ads}^{*ClO_4-H_2O} = G^{*ClO_4-H_2O} + 5G_{(aq)}^{H_2O} - G^{*6H_2O} - G_{(aq)}^{ClO_4^-} - n|e|U \quad D.18$$

which represents the energy of adsorption of a perchlorate ion on a surface covered with $2/3$ ML water molecules, perturbing the water adlayer and displacing water molecules after its adsorption. In our case, the adsorbed perchlorate is solvated with one water molecule.

D4 Adsorption free energies of *OH , *H and *O

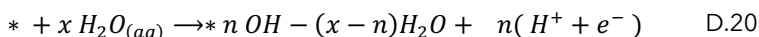
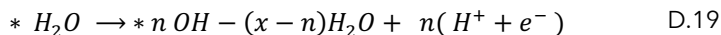
D4.1 Adsorption of hydroxyl and water adlayer

The adsorption energy of *OH was calculated within a explicit water bilayer. In this study we used a single water bilayer with a total water species coverage of $2/3$ ML, and varied the hydroxyl ($^*OH + ^*H_2O$) coverage by removing hydrogen from the adlayer. The water bilayer structure of $\sqrt{3} \times \sqrt{3} R30^\circ$ has been found to be stable on closed-packed metal surfaces.¹⁵⁻¹⁷ Furthermore, the good match between the lattice constant of metals and the water layer makes this model attractive for computational electrocatalysis as a good approximation to account for solvation effects,^{13,18-21} especially those coming from the first solvation shell.

**FIGURE D5**

Hydroxyl (*OH) free energy of adsorption as a function of coverage on Pd_{ML}Pt(111) calculated at the PBE and PBED3 levels of theory. The plotted adsorption energy is calculated with two different reference states: from the adsorbed water bilayer (*H₂O) and from solution-phase water (H₂O).

We can calculate the adsorption energy of *OH in two ways: (i) by using the adsorbed water bilayer as the reference state^{18,22} (i.e. using Eq. D.19), and (ii) by using solution-phase water as the reference state (i.e. using Eq. D.20).



In both cases $x = 6$. Figure D5 shows the adsorption energy of *OH as a function of *OH coverage calculated from either solution phase water (H₂O (aq)) or an adsorbed water bilayer (*H₂O) as reference state and with and without dispersion corrections for both cases. We observe that:

- 1) When referencing with respect to adsorbed water, for PBE and PBED3 the adsorption energies are basically the same and do not differ by more than 0.05 (± 0.02) eV, see Table D1 OH (b) and Figure D5 cyan (PBED3) and blue lines (PBE).
- 2) When referencing with respect to solution-phase water with PBE, the energies are less favorable (red triangles) than those calculated with PBED3 (velvet diamonds). The difference between these two at the lowest coverage is ~ 1.32 eV.
- 3) As the *OH coverage increases, the energies tend to converge and do not differ by more than ~ 0.2 eV, independent of the reference state.

Since the water-metal interactions are most affected by vdW interactions,^{23,24} the strong promotion of the adsorption of *OH + *H₂O at low *OH coverage, and

weaker promotion at high *OH coverage (relative to that calculated without vdW corrections) is simply proportional to the amount of water present in the *OH + *H₂O bilayer. This effect is roughly canceled when using an adsorbed water as the reference state.

Similarly to case 1, the adsorption thermodynamics of the water adlayer on Pt(111) relative to that on Pd_{ML}Pt(111) with vdW corrections does not significantly differ from that obtained without the vdW corrections. In fact, the difference in binding strength with vs. without vdW corrections between the two surfaces is ~0.03 eV, with stronger adsorption on Pd_{ML}Pt(111). This is because the stabilization incorporated by the vdW corrections for both surfaces is of the same magnitude, ~0.24 eV. Thus, the effect of including vdW corrections is also canceled when using adsorbed water as a reference state in the calculation of our adsorption potentials. In this way, the impact of vdW corrections is minimal as shown in Figure D5 on Pd_{ML}Pt(111). In either case, an appropriate representation of water adsorption is necessary for obtaining accurate DFT adsorption potentials.

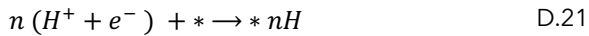
TABLE D1

Free energies of adsorption in eV for 1/3 ML coverage of *H, *O and 1/3*OH-1/3 *H₂O (PBE and PBED3). Using (a) solution-phase water and (b) adsorbed water bilayer as the reference state.

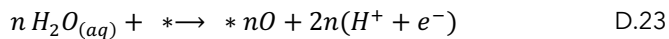
	PBE		PBED3	
	Pd _{ML} Pt(111)	Pt(111)	Pd _{ML} Pt(111)	Pt(111)
*H	-0.35	-0.29	-0.45	-0.39
*OH (a)	0.66	0.71	0.10	0.20
*OH (b)	0.37	0.43	0.35	0.39
*O	1.25	1.46	1.11	1.31

D4.2 Adsorption of hydrogen and oxygen

The free energies of adsorption of *H, *O were calculated at different coverages using the same 3×3 unit cell by the following equations:



$$\Delta G_{ads}^{*H} = \frac{G^{(*nH)} - \frac{n}{2} G_{(g)}^{H_2} - G^*}{n} \quad \text{D.22}$$



$$\Delta G_{ads}^{*O} = \frac{G^{*nO} + 2n \frac{1}{2} G_{(g)}^{H_2} - n G_{(aq)}^{H_2O} + G^*}{n} \quad \text{D.24}$$

where (*) is the surface, *H and *O are adsorbed species, n equals the number of adsorbed species per unit cell, and G^* is the free energy of the isolated slab. The adsorption of *H and *O were calculated at their most stable sites (fcc) in both cases, and without explicit solvation following Eqs. D.22 and D.24.

D5 Free energies vs. coverage diagrams

D5.1 Pd_{ML}Pt(111) Phase Diagrams

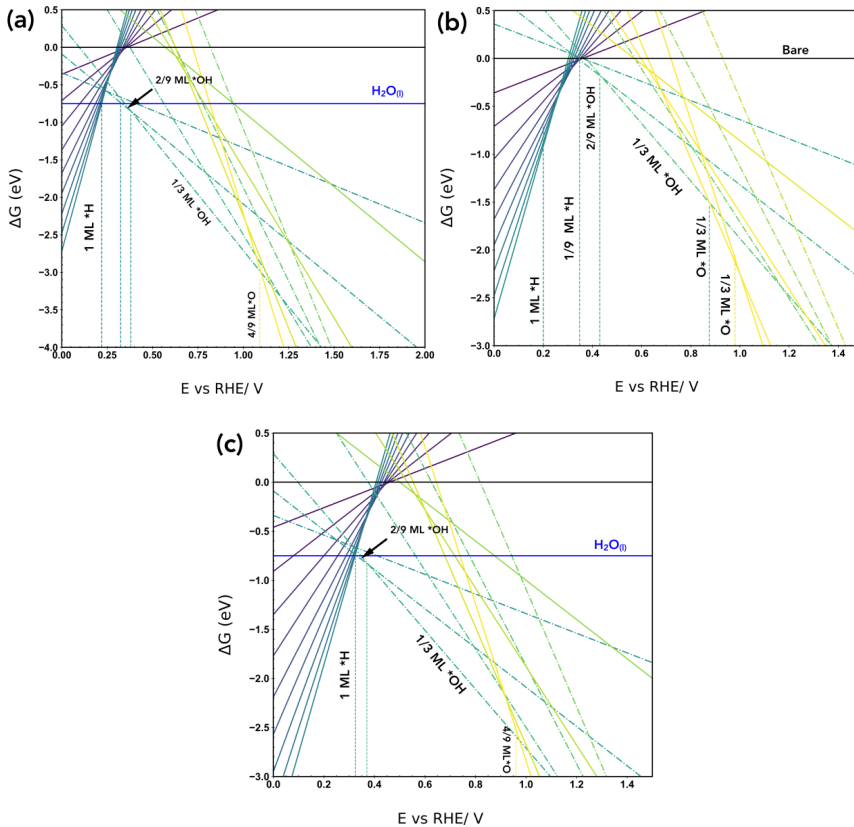
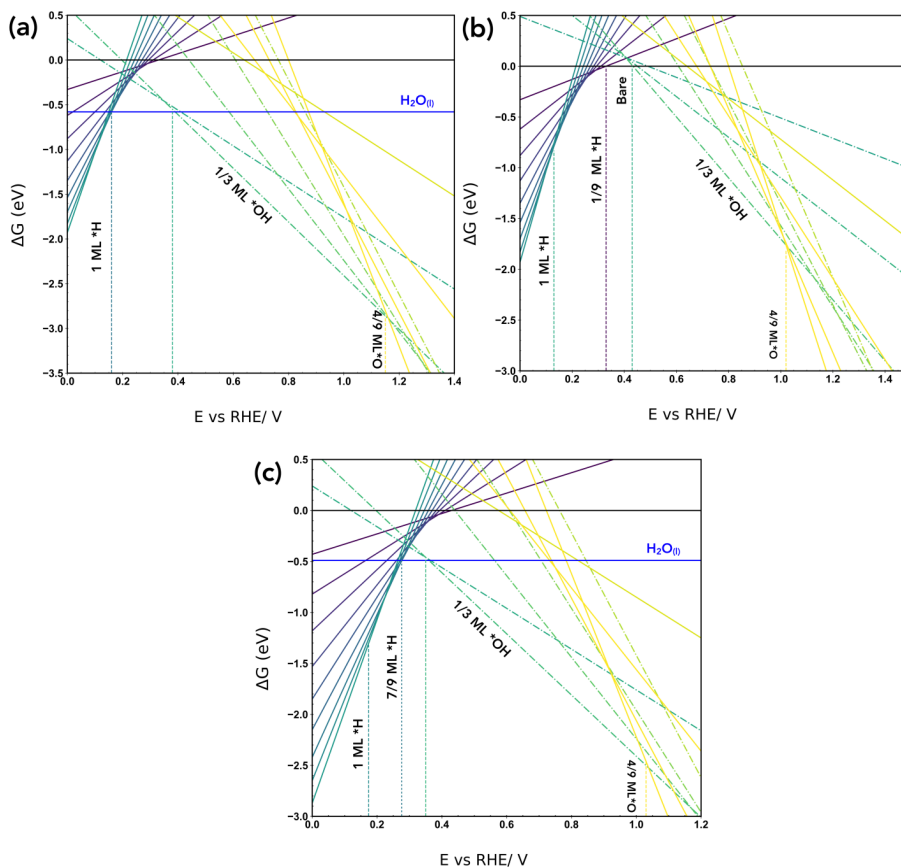


FIGURE D6

Calculated free energies of adsorption for Pd_{ML}Pt(111) as a function of potential vs RHE using three different methods. Method 1, shown in (a), where the adsorption potentials of hydroxyl are calculated from solution phase water with PBED3, as shown in Eq. D.20, while the adsorption potentials of hydrogen and oxygen are calculated with PBE. Method 2, shown in (b), the adsorption potentials are calculated with PBE and the reference state for *OH adsorption is the adsorbed water adlayer, as shown in Eq. D.19. Method 3, shown in (c), the adsorption potentials are calculated with PBED3 and solution phase water is used as the reference state, as shown in Eq. D.20.

D5.2 Pt(111) Phase Diagrams

**FIGURE D7**

Calculated free energies of adsorption for Pt(111) as a function of potential vs RHE using three different methods. Method 1, shown in (a), where the adsorption potentials of hydroxyl are calculated from solution phase water with PBED3, as shown in Eq. D.20, while the adsorption potentials of hydrogen and oxygen are calculated with PBE. Method 2, shown in (b), the adsorption potentials are calculated with PBE and the reference state for $*OH$ adsorption is the adsorbed water adlayer, as shown in Eq. D.19. Method 3, shown in (c), the adsorption potentials are calculated with PBED3 and solution phase water is used as the reference state, as shown in equation 20.

D6 References

- (1) Hoyer, R.; Kibler, L. A.; Kolb, D. M. The Initial Stages of Palladium Deposition onto Pt(1 1 1). *Electrochim. Acta* **2003**, *49* (1), 63-72.
- (2) *Thin Films: Preparation, Characterization, Applications*; Soriaga, M. P., Stickney, J., Bottomley, L. A., Kim, Y.-G., Eds.; Springer US, 2002.
- (3) Arenz, M.; Stamenkovic, V.; Schmidt, T. J.; Wandelt, K.; Ross, P. N.; Markovic, N. M. The Effect of Specific Chloride Adsorption on the Electrochemical Behavior of Ultrathin Pd Films Deposited on Pt(111) in Acid Solution. *Surf. Sci.* **2003**, *523* (1), 199-209.
- (4) Kresse, G.; Furthmüller, J. Efficient Iterative Schemes for Ab Initio Total-Energy Calculations Using a Plane-Wave Basis Set. *Phys. Rev. B* **1996**, *54* (16), 11169-11186.
- (5) Perdew, J. P.; Burke, K.; Ernzerhof, M. Generalized Gradient Approximation Made Simple. *Phys. Rev. Lett.* **1996**, *77* (18), 3865-3868.
- (6) Kresse, G.; Joubert, D. From Ultrasoft Pseudopotentials to the Projector Augmented-Wave Method. *Phys. Rev. B* **1999**, *59* (3), 1758-1775.
- (7) Monkhorst, H. J.; Pack, J. D. Special Points for Brillouin-Zone Integrations. *Phys. Rev. B* **1976**, *13* (12), 5188-5192.
- (8) Grimme, S.; Antony, J.; Ehrlich, S.; Krieg, H. A Consistent and Accurate Ab Initio Parametrization of Density Functional Dispersion Correction (DFT-D) for the 94 Elements H-Pu. *J. Chem. Phys.* **2010**, *132* (15), 154104.
- (9) Grimme, S.; Ehrlich, S.; Goerigk, L. Effect of the Damping Function in Dispersion Corrected Density Functional Theory. *J. Comput. Chem.* **2011**, *32* (7), 1456-1465.
- (10) Methfessel, M.; Paxton, A. T. High-Precision Sampling for Brillouin-Zone Integration in Metals. *Phys. Rev. B* **1989**, *40* (6), 3616-3621.
- (11) Chase, Jr., M. W.; Davies, C. A.; Downey, Jr., J. R.; Frurip, D. J.; MacDonald, R. A.; Syverud, A. N. NIST-JANAF Thermochemical Tables. *J. Phys. Chem. Ref. Data* **1985**, *Suppl. 1 to Vol. 14*, 1856.
- (12) Fultz, B. Vibrational Thermodynamics of Materials. *Prog. Mater. Sci.* **2010**, *55*, 247-352.
- (13) Nørskov, J. K.; Rossmeisl, J.; Logadottir, A.; Lindqvist, L.; Kitchin, J. R.; Bligaard, T.; Jónsson, H. Origin of the Overpotential for Oxygen Reduction at a Fuel-Cell Cathode. *J. Phys. Chem. B* **2004**, *108* (46), 17886-17892.
- (14) Calle-Vallejo, F.; Koper, M. T. M. First-Principles Computational Electrochemistry: Achievements and Challenges. *Electrochim. Acta* **2012**, *84* (Supplement C), 3-11.
- (15) Ogasawara, H.; Brena, B.; Nordlund, D.; Nyberg, M.; Pelmenschikov, A.; Pettersson, L. G. M.; Nilsson, A. Structure and Bonding of Water on Pt(111). *Phys. Rev. Lett.* **2002**, *89* (27), 276102.
- (16) Schnur, S.; Groß, A. Properties of Metal-Water Interfaces Studied from First Principles. *New J. Phys.* **2009**, *11* (12), 125003.
- (17) Michaelides, A.; Hu, P. Catalytic Water Formation on Platinum: A First-Principles Study. *J. Am. Chem. Soc.* **2001**, *123* (18), 4235-4242.

- (18) He, Z.-D.; Hanselman, S.; Chen, Y.-X.; Koper, M. T. M.; Calle-Vallejo, F. Importance of Solvation for the Accurate Prediction of Oxygen Reduction Activities of Pt-Based Electrocatalysts. *J. Phys. Chem. Lett.* **2017**, *8* (10), 2243-2246.
- (19) McCrum, I. T.; Janik, M. J. PH and Alkali Cation Effects on the Pt Cyclic Voltammogram Explained Using Density Functional Theory. *J. Phys. Chem. C* **2016**, *120* (1), 457-471.
- (20) Roman, T.; Groß, A. Structure of Water Layers on Hydrogen-Covered Pt Electrodes. *Catal. Today* **2013**, *202* (Supplement C), 183-190.
- (21) Granda-Marulanda, L. P.; Builes, S.; Koper, M. T. M.; Calle-Vallejo, F. Influence of Van Der Waals Interactions on the Solvation Energies of Adsorbates at Pt-Based Electrocatalysts. *ChemPhysChem* **2019**, *0* (0).
- (22) McCrum, I. T.; Hickner, M. A.; Janik, M. J. First-Principles Calculation of Pt Surface Energies in an Electrochemical Environment: Thermodynamic Driving Forces for Surface Faceting and Nanoparticle Reconstruction. *Langmuir* **2017**, *33* (28), 7043-7052.
- (23) Forster-Tonigold, K.; Groß, A. Dispersion Corrected RPBE Studies of Liquid Water. *J. Chem. Phys.* **2014**, *141* (6), 064501.
- (24) Carrasco, J.; Klimeš, J.; Michaelides, A. The Role of van Der Waals Forces in Water Adsorption on Metals. *J. Chem. Phys.* **2013**, *138* (2), 024708.

E: Supporting Information for Chapter 6

E1 Experimental Details

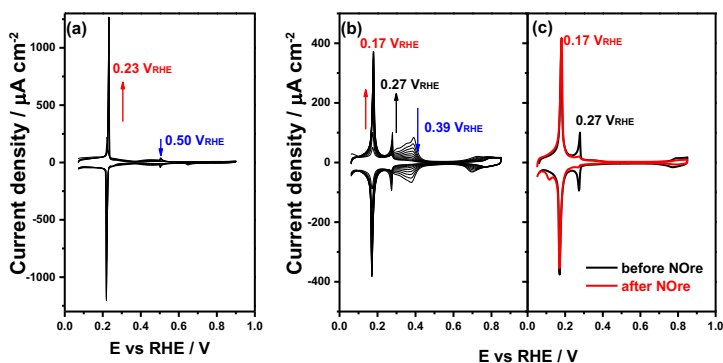
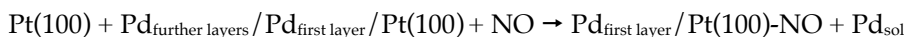


FIGURE E1

Cyclic voltammograms for (a) Pt(111) and (b) Pt(100) in 0.1 M H_2SO_4 + 0.1 mM PdSO_4 , recorded in successive stages during Pd deposition experiment. Scan rate: 50 mV s^{-1} . Arrows indicate the evolution with time. (c) Stable cyclic voltammograms of Pd/Pt(100) electrode in 0.1 M H_2SO_4 before NO adsorption and reductive stripping (black line) and the same Pd/Pt(100) electrode in 0.1 M H_2SO_4 after NO adsorption and reductive stripping (red line).

Figure E1a shows the effect of the progressive accumulation of palladium on the voltammetric profile of Pt(111) electrode during the electrochemical deposition of palladium monolayer. At the shortest deposition times, the presence of palladium on the surface is reflected in the growth of a sharp adsorption state at $0.23 \text{ V}_{\text{RHE}}$, simultaneously with the progressive decrease of the characteristic adsorption states of Pt(111) in 0.1 M H_2SO_4 . In addition, the presence of the characteristic spike of Pt(111) at $0.50 \text{ V}_{\text{RHE}}$ strongly suggests the existence of wide Pt(111) domains. Increasing deposition cycles lead to the contributions from the Pt(111) domains around $0.50 \text{ V}_{\text{RHE}}$ to become blocked progressively. A previous study using in situ scanning tunnelling microscopy (STM) showed an complete pseudomorphic monolayer of Pd is formed prior to bulk deposition during electrochemical deposition of Pd on Pt(111).¹ The voltammetric charge of (bi)sulfate adsorption at $0.23 \text{ V}_{\text{RHE}}$ can be related in a quantitative way to the palladium coverage and increases to a charge value of $320 \mu\text{C cm}^{-2}$ for $\text{Pd}_{\text{ML}}\text{Pt}(111)$.^{2,3}

Figure E1b shows the characteristic adsorption peak of Pt(100) electrode at 0.39 V_{RHE} progressively diminishes whereas a new sharp adsorption state appears at 0.17 V_{RHE}. The experimental result is interpreted as the progressive blocking of the Pt(100) substrate sites by a first monolayer of palladium atoms directly deposited on the Pt(100) substrate. As the deposition continues a new feature appears at 0.27 V_{RHE} while the peak at 0.39 V_{RHE} corresponding to the remaining Pt(100) unblocked sites has not been completely suppressed. The appearance of a second adsorption state at 0.27 V_{RHE} for palladium deposited on Pt(100) substrates is associated to the growth of palladium in second, third and further layers. The easiest way to obtain a Pt(100) electrode fully covered by a single palladium monolayer is to deposit palladium until all the Pt(100) sites are blocked and then remove the excess by the NO treatment described above:⁴



in which Pd_{first layer} means palladium adatoms in the first monolayer, Pd_{further layers} is the second and multilayers, and Pd_{sol} represents stable palladium species in solution.

Figure E1c shows the final voltammogram in 0.1 M H₂SO₄ (red line): a characteristic peak at 0.17 V_{RHE} related to the (bi)sulfate anion adsorption on Pd monolayer is observed, the contributions assigned to the second stage of Pd deposition at 0.27 V_{RHE} and uncovered Pt(100) electrode domain at 0.39 V_{RHE} have been eliminated. The voltammogram of Pd_{ML}Pt(100) is stable upon successive cycles, suggesting that the monolayer does not undergo further modification.

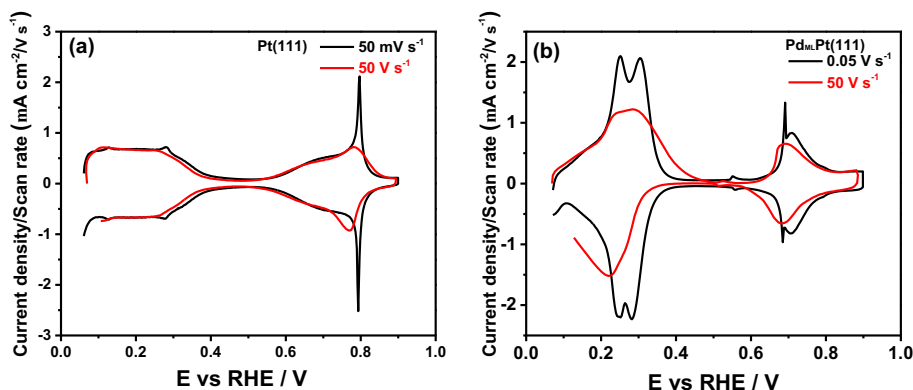
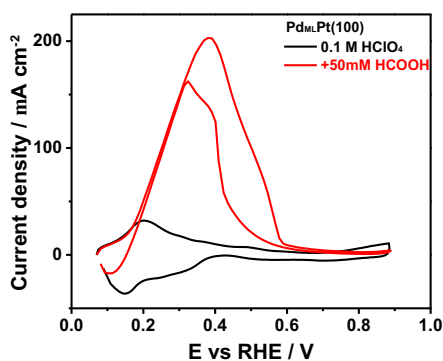


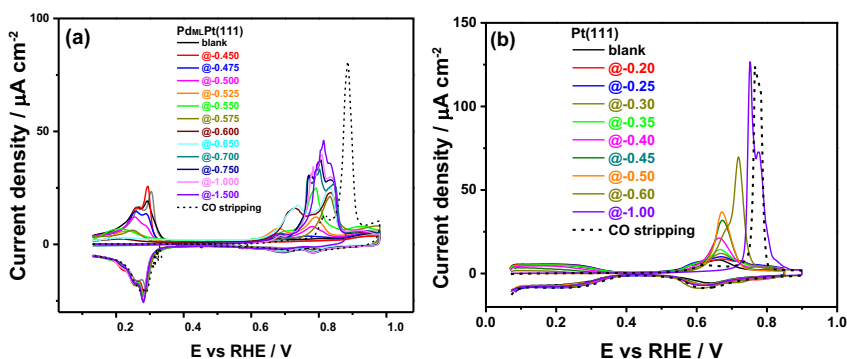
FIGURE E2

Voltammograms of (a) Pt(111) and (b) Pd_{ML}Pt(111) electrode in 0.1 M HClO₄ recorded at 0.05 V s⁻¹ (black line) and 50 V s⁻¹ (red line), resp.

**FIGURE E3**

Voltammograms of Pd_{ML}Pt(100) electrode in 0.1 M HClO₄ (black line) and 0.1 M HClO₄ + 50 mM HCOOH, recorded at 50 V s⁻¹.

Figure E4 shows the oxidation of formic acid on Pd_{ML}Pt(100) electrode in 0.1 M HClO₄ + 50 mM HCOOH at a high scan rate of 50 V s⁻¹. The current corresponding to the oxidation of formic acid process is much larger than the current corresponding to the reversible formate adsorption/desorption so that this latter contribution cannot be separated from the voltammogram. The results suggest a much faster kinetics of formic acid oxidation reaction on Pd_{ML}Pt(100) than that on Pd_{ML}Pt(111) electrode.

**FIGURE E4**

Voltammograms for the oxidative stripping of CO adlayer produced on (a) Pd_{ML}Pt(111) and (b) Pt(111) electrode after doing CO₂ reduction at different vertex potentials in pH=3.0 (0.001M HClO₄/0.099M KClO₄) solution saturated with CO₂, recorded at 10 mV s⁻¹. A CO stripping experiment result (dashed line) of a saturated CO adlayer is performed under identical condition for comparison.

Figure E5 shows the voltammograms for the oxidative stripping of CO adlayer produced during CO₂ reduction on the Pd_{ML}Pt(111) and Pt(111) electrode, resp. Figure E5a shows anodic peaks between 0.650 and 0.900 V_{RHE} are observed when doing CO₂ reduction on the Pd_{ML}Pt(111) electrode by increasing the vertex potential in steps of 0.025 V from -0.475 V_{RHE}. These anodic peaks correspond to the oxidation of adsorbed CO formed during CO₂ reduction. It is reasonable to assume that there is no CO formation from CO₂ reduction on Pd_{ML}Pt(111) surface at lower overpotentials than that of -0.475 V_{RHE}. In Figure E4a, the production of the CO is shown to increase with increasing the overpotential for CO₂ reduction: for the overpotential of -0.475, -0.500, -0.525, -0.550, -0.575, -0.600, -0.650, -0.700 and -0.750 V_{RHE}, the coverage of CO adlayer is 0.13, 0.19, 0.22, 0.29, 0.31, 0.52, 0.58, 0.71 and 0.72 ML, resp. As can be seen from Figure E4a, the onset potential and shape of CO adlayer oxidation peak on the Pd_{ML}Pt(111) electrode strongly depends on its coverage. The full CO adlayer is stripped off at 0.90 V_{RHE} (dashed line); such a high coverage is not obtained during CO₂ reduction. The subsequent scan indicates the entire CO adlayer on Pd_{ML}Pt(111) electrode was stripped in a single positive-going sweep and retains the well-defined hydrogen adsorption and anion desorption features in the low-potential region. In the case of the Pt(111) electrode, reducing CO₂ to adsorbed CO starts at -0.25 V_{RHE} and the surface is poisoned when the negative vertex potential reaches -0.60 V_{RHE}. Figure E4b shows that with increasing overpotential for CO₂ reduction on Pt(111), the formation of the CO increases: for the overpotential of -0.25, -0.30, -0.35, -0.40, -0.50, -0.60 and -1.0 V_{RHE}, the coverage of CO adlayer is 0.23, 0.37, 0.37, 0.47, 0.59, 0.63 and 0.66 ML, resp. The subsequent scan shows the recovery of the Pt(111) surface after the CO adlayer oxidation.

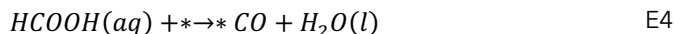
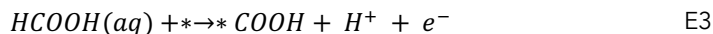
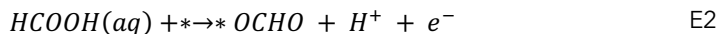
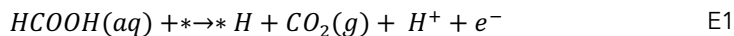
E2 Computational Details

E2.1 Free energies calculations

The formation free energies of adsorbed *H, *CO, *OCHO and *COOH were calculated from formic acid in solution, (HCOOH (aq)) for the formic acid oxidation reaction, and from carbon dioxide in gas-phase, (CO₂ (g)), protons and electrons, for the CO₂ reduction reaction. Below we show how the free energies are calculated in both cases.

E2.2 Formic Acid oxidation

The following chemical equations show how the formation free energies of the different adsorbates are calculated for formic acid oxidation.



where, * represents the adsorption site. The free energies of adsorption are then calculated as shown below

$$G_{*H}^{ads} = G_{*H} + G_{CO_2(g)} + \frac{1}{2}G_{H_2(g)} - G_{HCOOH(aq)} - G_* \quad E5$$

$$G_{*OCHO}^{ads} = G_{*OCHO} + \frac{1}{2}G_{H_2(g)} - G_{HCOOH(aq)} - G_* \quad E6$$

$$G_{*COOH}^{ads} = G_{*COOH} + \frac{1}{2}G_{H_2(g)} - G_{HCOOH(aq)} - G_* \quad E7$$

$$G_{*CO}^{ads} = G_{*CO} + G_{H_2O(l)} - G_{HCOOH(aq)} - G_* \quad E8$$

Each free energy is calculated as $G = EDFT + ZPE + TS$, where EDFT is the energy obtained from the DFT calculation at 0K, ZPE is the zero-point energy determined from the vibrational frequencies obtained using the harmonic-oscillator approximation. The TS is the temperature at $T = 298.15$ K times the entropy (S) term containing i) all the contributions (translational, rotational and vibrational) for the free energies of species in the gas phase and is taken from standard thermodynamic tables⁵ and ii) for the free energies of adsorbed species containing vibrational contributions. The free energy of the surface, G_* , is the energy from DFT at 0 K. The free energies of $CO_2(g)$ and $CO(g)$ are corrected by -0.19 and 0.24 eV, these corrections come from the difference between the experimental standard free energy of formation ΔG_{EXP}° and the DFT formation energy ΔG_{DFT}° , as PBE does not describe well their formation energies.⁶⁻⁸

E2.3 Free energy of solution phase HCOOH (aq)

The solution phase free energy of HCOOH (aq) was calculated using the SHE equilibrium redox potential of $\text{CO}_2(\text{g}) + 2\text{H}^+ + 2\text{e}^- \rightarrow \text{HCOOH}(\text{aq})$, $E^\circ = -0.11 \text{ V vs SHE}$,⁹ where the free energy of $\text{CO}_2(\text{g})$ is calculated within DFT. This was used to solve for the standard free energy of formic acid in solution phase, $\Delta G_{\text{HCOOH}}^\circ(\text{aq})$ and ultimately to solve for the aqueous free energy at the experimental conditions, see below.

$$\Delta G_{\text{HCOOH}}^\circ(\text{aq}) = G_{\text{CO}_2(\text{g})}^\circ + 2G_{\text{H}^+}^\circ - 2|e|U \quad \text{E9}$$

where $U = E^\circ = -0.11 \text{ V}$,⁹ and $G_{\text{H}^+}^\circ = \frac{1}{2}G_{\text{H}_2(\text{g})}^\circ$ at 0 V in the SHE scale.

The standard solution phase free energy, $\Delta G_{\text{HCOOH}}^\circ(\text{aq})$, was then used to obtain the free energy of formic acid, ΔG_{HCOOH} , at the experimental conditions of 0.1M HClO_4 and 50 mM HCOOH, following the Nernst equation.

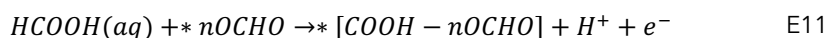
$$\Delta G_{\text{HCOOH}} = \Delta G_{\text{HCOOH}}^\circ(\text{aq}) + k_b T \ln(Cf) \quad \text{E10}$$

Cf is the actual concentration of HCOOH and is obtained using the pKa of formic acid, 3.94 and the starting concentrations of HClO_4 and HCOOH.

The free energies of the protons and electrons as expressed in the adsorption reactions, equations 1 to 4, were calculated using the computational hydrogen electrode (CHE) model.¹⁰

E2.4 Formate coadsorption with *H, *CO and *COOH

To investigate the effect of formate coverage on the free energy of formation of adsorbed *H, *CO and *COOH we calculated the energies from HCOOH (aq) and n molecules of formate *OCHO adsorbed on the surface. For example, the adsorption of *COOH at different formate coverages is calculated using the following chemical reaction



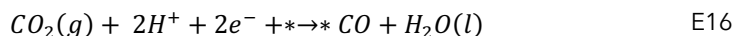
and its free energy of adsorption

$$G_{\text{*COOH-nOCHO}}^{\text{ads}} = G_{\text{*COOH-nOCHO}} + \frac{1}{2}G_{\text{H}_2(\text{g})}^\circ - G_{\text{HCOOH}(\text{aq})} - G_{n \text{*OCHO}} \quad \text{E12}$$

with $n = 1-3$ using the 3x3 unit cell representing coverages of 0.11ML to 0.33 ML and with $n = 1$ using the 2x2 unit cell to represent coverages of 0.25 ML. * $[\text{COOH-nOCHO}]$ means both COOH and n OCHO are adsorbed in the same unit cell.

E2.5 CO₂ Reduction

Similarly, the adsorption energetics were calculated for the reduction reaction, i.e. the production of formic acid from CO₂. This time the reference state is based on CO₂ (g), protons, and electrons. All the gas-phase corrections for CO₂(g) and CO (g) are included as discussed above, and the CHE model is used for the coupled proton and electron transfer.



The free energies of adsorption are then calculated as shown below.

$$G_{*H}^{ads} = G_{*H} - \frac{1}{2}G_{H_2(g)} - G_* \quad \text{E17}$$

$$G_{*OCHO}^{ads} = G_{*OCHO} - G_{CO_2(g)} - \frac{1}{2}G_{H_2(g)} - G_* \quad \text{E18}$$

$$G_{*COOH}^{ads} = G_{*COOH} - G_{CO_2(g)} - \frac{1}{2}G_{H_2(g)} - G_* \quad \text{E19}$$

$$G_{*CO}^{ads} = G_{*CO} + G_{H_2O(l)} - G_{CO_2(g)} - G_{H_2(g)} - G_* \quad \text{E20}$$

The limiting potentials for the first protonation step during CO₂ reduction reaction to *COOH are calculated at the potential when the $G_{*COOH}^{ads} = 0$ as show in Eq.E23



$$G_{*COOH}^{ads} = G_{*COOH} - G_{CO_2(g)} - \frac{1}{2}G_{H_2(g)} - G_* + |e|U \quad \text{E22}$$

$$U = \frac{G(CO_2 g) + \frac{1}{2}G(H_2(g)) + G_*COOH + G(*)}{1|e|} \quad \text{E23}$$

Table E1 shows the free energies adsorption for $^*\text{COOH}$, the precursor of $^*\text{CO}$, with H-up and H-down (see Figure E6), calculated from $\text{HCOOH}(\text{aq})$, Eq. E7, and from $\text{CO}_2(\text{g})$, Eq. E19, at $1/9$ ML coverage on $\text{Pd}_{\text{ML}}\text{Pt}(111)$, $\text{Pt}(111)$ and $\text{Pd}(111)$.

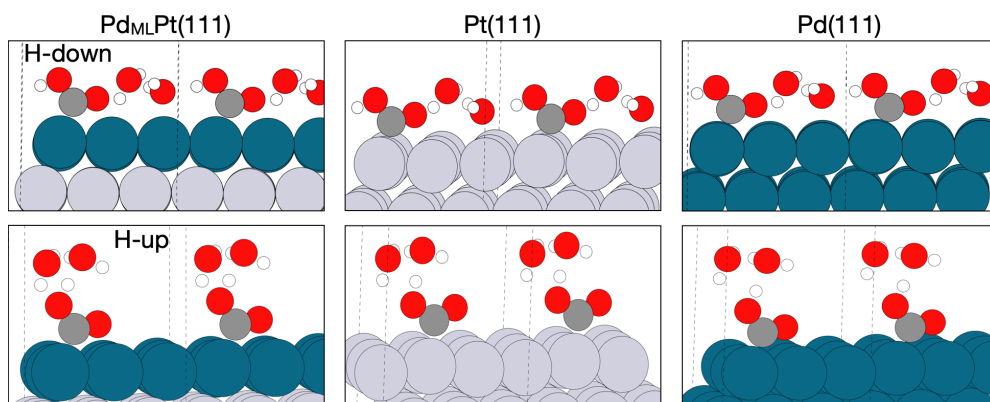


FIGURE E5:

Illustration of $^*\text{COOH}$ solvated with two explicit water molecules with hydrogen down (H-down) and hydrogen up (H-up) configuration on the $\text{Pd}_{\text{ML}}\text{Pt}(111)$, $\text{Pt}(111)$, and $\text{Pd}(111)$ surfaces. The boundary of the unit cell is delineated by the vertical dashed line, and each Figure E shows two-unit cells of 3×3 .

TABLE E1

Free energies of adsorption for solvated $^*\text{COOH}$ with H-up and H-down configuration at $1/9$ ML coverage calculated for formic acid oxidation reaction, and for CO_2 reduction reaction, where $\text{HCOOH}(\text{aq})$ or $\text{CO}_2(\text{g})$ are the reference state respectively. Energies are in eV.

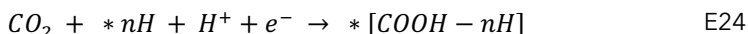
	$\text{Pd}_{\text{ML}}\text{Pt}(111)$	$\text{Pt}(111)$	$\text{Pd}(111)$
$\text{COOH}_{\text{up-sol}}$ from $\text{HCOOH}(\text{aq})$	-0.15	-0.48	-0.10
$\text{COOH}_{\text{down-sol}}$ from $\text{HCOOH}(\text{aq})$	-0.37	-0.63	-0.29
$\text{COOH}_{\text{up-sol}}$ from $\text{CO}_2(\text{g})$	-0.003	-0.34	0.04
$\text{COOH}_{\text{down-sol}}$ from $\text{CO}_2(\text{g})$	-0.23	-0.49	-0.15

E2.6 Effect of hydrogen coverage on the free energy of $^*\text{COOH}$

We investigated the influence of the hydrogen coverage on the adsorption energy of $^*\text{COOH-sol}$, the precursor of $^*\text{CO}$ formation, on the three different surfaces. The energy of $^*\text{COOH-sol}$ is described further below in the solvation effects section. Basically, the

solvation energy is added to the free energies of the systems in vacuum. The free energies were calculated following the equations below, $*nH$ represents the surface with n number of adsorbed hydrogens per unit cell. The hydrogen coverages investigated were 1/3 ML and 1ML.

From Figure E6 we can see that the effect of hydrogen coverage on the adsorption energy of $*COOH$ -sol is a decrease in its binding energy, as expected due to repulsion interactions, but comparing between the three surfaces $*COOH$ -sol adsorbs on Pt(111) stronger.



$$G_{*[COOH-nH]}^{ads} = G_{*[COOH-nH]} - G_{CO_2} - G_{*nH} - \frac{1}{2}G_{H_2(g)} \quad E25$$

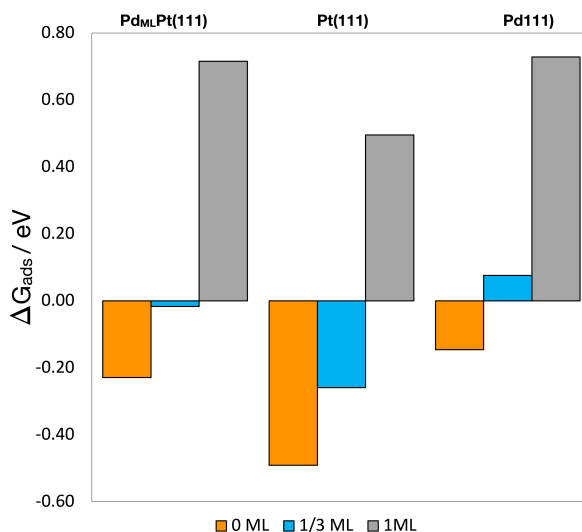


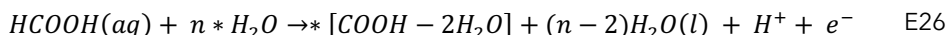
FIGURE E6

Free energy of formation of adsorbed $*COOH$ in the absence (orange) and presence of different coverages of coadsorbed hydrogen at 1/3 ML (blue) and 1 ML (grey) on Pd_{ML}Pt(111), Pt(111) and Pd(111) at 0 V vs RHE, the solvation energy is added to $*COOH$ in all cases as explained in the solvation effects section.

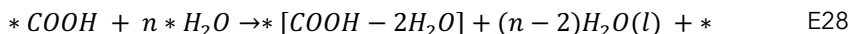
E2.7 Solvation effects

E2.7.1 Solvation effect on *COOH

We consider the effect of solvation on the adsorption of *COOH by solvating *COOH with 2 explicit water molecules, named as *COOH-sol. Adsorbed water bilayer and solution-phase formic acid were used as the reference states, see Eq. E26 for formic acid oxidation, while for the reduction reaction we use adsorbed water, CO₂ (g), and protons and electrons, Eq. E27. The adsorbed water reference state is the adsorbed water in the ice-like structure in a 3x3 unit cell, while in 2x2 unit cell we used a reference state of 4 adsorbed hydrogen bonded water molecules. The following equations correspond to n=6 in the 3x3 unit cell and n=4 in the 2x2 unit cell.



The solvation energy of adsorbed *COOH, Ω_{*COOH} , is the difference between the non-solvated and solvated free energies of *COOH. That difference gives Eq. E28 and the solvation energy is Eq. E29



$$\Omega_{*COOH} = G_{*[COOH-2H_2O]} + (n - 2)G_{H_2O(l)} + G_* - G_{*COOH} - n G_{*H_2O} \quad E29$$

The solvation energy, Ω_{*COOH} , calculated here is an estimate to capture the effect of solvation of coadsorbed *COOH with *OCHO, that is *[COOH-nOCHO], and to capture the effect of coadsorbed *COOH with hydrogen *[COOH-nH]. To account for such solvation effects, the solvation energy is added to the final free energy as, $G_{*[COOH-nOCHO]}^{ads} + \Omega_{*COOH}$, and $G_{*[COOH-nH]}^{ads} + \Omega_{*COOH}$ and represents an upper bound estimate of the solvation effect.

Table E2 shows the solvation energies determined for *COOH with H-up and H-down configuration at both 1/9 ML and 1/4 ML coverages on Pd_{ML}Pt(111), Pt(111) and Pd(111) surfaces. We determine 3 different solvation energies following Eq. E29. For example, H-down vac to Hup-sol, means that the reference state (*COOH) is adsorbed *COOH with hydrogen down configuration in vacuum (H-down vac), and the solvated *COOH is with hydrogen in the up configuration (Hup-sol). At high coverages 1/4 ML *COOH, higher stabilization (more negative solvation energies) is achieved for the *COOH with H up

configuration, while at low coverages higher stabilization is achieved for H down-vac to H down-sol. The reason for this might be more predominant repulsive interactions than solvation stabilization at higher coverages than at low coverages.

TABLE E2

Calculated solvation energies for *COOH adsorbate on Pd_{ML}Pt(111), Pt(111), Pd(111), at 1/9 ML and 1/4 ML coverages following Eq. E29. The solvation energies were calculated following different positions of the hydrogen on *COOH, where the H of the OH group could be on the H-down position or up.

<i>3x3-111 (1/9 ML)</i>	<i>Pd_{ML}Pt(111)</i>	<i>Pt(111)</i>	<i>Pd(111)</i>
<i>H down vac to H up-sol</i>	-0.30	-0.47	-0.35
<i>H up vac to H up-sol</i>	-0.38	-0.59	-0.46
<i>H down vac to H down-sol</i>	-0.53	-0.62	-0.54
<i>2x2-111 (1/4 ML)</i>	<i>Pd_{ML}Pt(111))</i>	<i>Pt(111)</i>	<i>Pd(111)</i>
<i>H down vac to H up-sol</i>	-0.17	-0.20	-0.28
<i>H up vac to H up-sol</i>	-0.33	-0.44	-0.42
<i>H down vac to H down-sol</i>	-0.13	-0.12	-0.29

In summary, *COOH is preferably adsorbed with a H-down type configuration at least up to 0.25 ML coverage of formate. Once the coverage of formate is increased to 0.33ML, *COOH with H-up configuration is more favorable. Therefore, in the coadsorbed system, where *COOH is co-adsorbed with 0.33 ML of *OCHO, we corrected for solvation with the solvation energy determined for the *COOH with H-up configuration.

*COOH coadsorbed with 1ML of hydrogen prefers to adsorb with H down configuration. For Pd and Pd_{ML}Pt(111) it is ~0.2 eV more favorable than H-down, while for Pt (111) is more favorable by ~ 0.04 eV. Therefore, we corrected the energy of the coadsorbed system with the solvation energy determined for *COOH with H-down configuration.

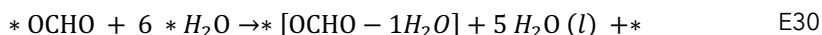
Again, these solvation corrections are an upper bound estimation of the solvation effect on *COOH.

E2.7.2 Solvation on *OCHO

Formate retains partial negative charge upon adsorption; to assess whether or not adsorbed formate might benefit from solvation, we determine its solvation energy with 1, 2, and 3 explicit water molecules following the assessment described in ref ¹¹. Briefly, the adsorbate in question can benefit from solvation via hydrogen bonding if the

difference between solvation energy with (n) number of water molecules and (n-1) is more negative than the water-self solvation energy on that surface, $\Omega^n - \Omega^{n-1} \leq \Omega_{H_2O}$, (where, Ω , refers to solvation energy). The water-self solvation energy was calculated as the difference in free energy between one water molecule at 1/9 ML and a water molecule within the water bilayer at 2/3 ML coverage. For Pt(111) that difference is -0.29 eV, for Pd_{ML}Pt(111) it is -0.18 eV and for Pd it is -0.14 eV. From column $\Delta 2 w-1w$ in Table E3, the difference in solvation energies of formate with two and one water molecules is higher than the water self-solvation, on all surfaces respectively, suggesting that solvation with one water molecule is enough. This solvation energy is an upper bound estimation of the solvation effect on formate.

The reference state to calculate the solvation energy is the adsorbed water bilayer in the 3x3 (111) unit cell, at 2/3 ML coverage, Eq. E30, and the solvation energy is the difference between the free energy of the solvated formate and the non-solvated formate, Ω_{*OCHO} , Eq. E31.



$$\Omega_{*OCHO} = G_{*[OCHO-1H_2O]} + 5G_{H_2O(l)} + G_* - G_{*OCHO} - 6 G_{*H_2O} \quad E31$$

TABLE E3:

Calculated solvation energies for adsorbed formate at 1/9 ML with 1, 2, and 3 water molecules. Last two columns show the difference between, 2 H₂O molecules (2w) and 1 H₂O molecules, and between 3 H₂O (3w) and 2 H₂O molecules.

Surface	1 H ₂ O	2 H ₂ O	3 H ₂ O	$\Delta 2 w-1w$	$\Delta 3 w-2w$
Pd _{ML} Pt(111)	-0.50	-0.27	-0.24	0.23	0.03
Pt(111)	-0.39	-0.23	--	0.16	--
Pd(111)	-0.51	-0.25	-0.24	0.26	0.01

E2.8 Dipole moments and Bader partial charges

Bader partial charge analysis was performed with the Atoms in Molecules, AIM, Bader analysis,^{12,13} using the Bader program from Henkelman's group.¹⁴

TABLE E4

Dipole moments and Bader partial charges for various adsorbates on Pd_{ML}Pt(111), Pt(111) and Pd(111) at 1/9 ML coverage unless specified otherwise. [a] Total partial Bader charge of hydrogens adsorbed on the surface on the fcc sites, and [b] partial Bader charge of only *COOH.

adsorbate	$\Delta\mu / e \cdot \text{\AA}$			$ q / e^-$		
	Pd _{ML} Pt(111)	Pt(111)	Pd(111)	Pd _{ML} Pt(111)	Pt(111)	Pd(111)
<i>H-fcc</i>	0.02	-0.01	0.01	-0.09	-0.03	-0.08
<i>H-top</i>	0.03	-0.03	0.02	0.00	0.04	0.00
<i>CO</i>	0.18	-0.03	0.17	-0.23	-0.01	-0.22
<i>OCHO</i>	-0.06	-0.23	-0.07	-0.50	-0.40	-0.48
<i>COOH- H up</i>	-0.24	-0.16	-0.25	-0.22	-0.16	-0.19
<i>COOH- H down</i>	0.06	0.21	0.06	-0.14	0.01	-0.10
<i>COOH-Hup sol</i>	-0.23	-0.18	-0.29	-0.20	-0.12	-0.17
<i>COOH-Hdown sol</i>	0.06	-0.35	-0.17	-0.15	-0.08	-0.11
<i>OCHO-sol</i>	-0.25	-0.41	-0.24	-0.58	-0.39	-0.39
<i>1/3 ML Hads-fcc</i>	0.06	-0.03	0.04	-0.25	-0.06	-0.21
<i>1 ML Hads-fcc</i>	0.09	-0.17	0.06	-0.56	-0.07	-0.51
^a <i>1/3 ML *H in *COOH</i>	0.12	0.18	0.15	-0.19	-0.05	-0.19
^a <i>1 ML *H in *COOH</i>	0.24	0.05	0.20	-0.61	-0.05	-0.48
^b <i>*COOH in 1/3 ML *H</i>	--	--	--	-0.08	-0.01	-0.04
^b <i>*COOH in 1 ML *H</i>	--	--	--	0.03	0.02	0.07

E2.9 Work functions

Work functions, Φ , were determined as, $\Phi = V - E_{Fermi}$, the difference between the Fermi energy and the one electron potential in vacuum.

TABLE E5

Calculated work function for the bare surfaces, Pd_{ML}Pt(111), Pt(111) and Pd(111), and at different hydrogen coverages.

	Φ/eV		
	Pd _{ML} Pt(111)	Pt(111)	Pd(111)
<i>Bare</i>	5.14	5.74	5.29
<i>1/9 ML</i>	5.20	5.71	5.32
<i>1/3 ML</i>	5.33	5.64	5.37
<i>1ML</i>	5.45	5.20	5.42

E3 References

1. Wakisaka, M., Asizawa, S., Uchida, H. & Watanabe, M. In situ STM observation of morphological changes of the Pt(111) electrode surface during potential cycling in 10 mM HF solution. *Phys. Chem. Chem. Phys.* **12**, 4184–4190 (2010).
2. Álvarez, B., Climent, V., Rodes, A. & Feliu, J. M. Anion adsorption on Pd-Pt(111) electrodes in sulphuric acid solution. *J. Electroanal. Chem.* **497**, 125–138 (2001).
3. Soriaga, M., Stickney, J., Bottomley, L. & Kim, Y. *Thin Films: Preparation, Characterization, Applications*. (Springer US, 2002).
4. Álvarez, B., Berná, A., Rodes, A. & Feliu, J. M. Electrochemical properties of palladium adlayers on Pt(100) substrates. *Surf. Sci.* **573**, 32–46 (2004).
5. Chase, Jr., M. W. *et al.* NIST-JANAF Thermochemical Tables. *J. Phys. Chem. Ref. Data Suppl.* **1 to Vol. 14**, 1856 (1985).
6. Peterson, A. A., Abild-Pedersen, F., Studt, F., Rossmeisl, J. & Nørskov, J. K. How copper catalyzes the electroreduction of carbon dioxide into hydrocarbon fuels. *Energy Environ. Sci.* **3**, 1311–1315 (2010).
7. Christensen, R., Hansen, H. A. & Vegge, T. Identifying systematic DFT errors in catalytic reactions. *Catal. Sci. Technol.* **5**, 4946–4949 (2015).
8. Granda-Marulanda, L. P. *et al.* A Semiempirical Method to Detect and Correct DFT-Based Gas-Phase Errors and Its Application in Electrocatalysis. *ACS Catal.* **10**, 6900–6907 (2020).
9. Bratsch, S. G. Standard Electrode Potentials and Temperature Coefficients in Water at 298.15 K. *J. Phys. Chem. Ref. Data* **18**, 1–21 (1989).
10. Nørskov, J. K. *et al.* Origin of the Overpotential for Oxygen Reduction at a Fuel-Cell Cathode. *J. Phys. Chem. B* **108**, 17886–17892 (2004).
11. Rendón-Calle, A., Builes, S. & Calle-Vallejo, F. Substantial improvement of electrocatalytic predictions by systematic assessment of solvent effects on adsorption energies. *Appl. Catal. B Environ.* **276**, 119147 (2020).
12. Bader, R. F. W. *Atoms in molecules: a quantum theory*. (Clarendon Press, 1994).
13. Bader, R. F. W. Atoms in molecules. *Acc. Chem. Res.* **18**, 9–15 (1985).
14. Henkelman, G., Arnaldsson, A. & Jónsson, H. A fast and robust algorithm for Bader decomposition of charge density. *Comput. Mater. Sci.* **36**, 354–360 (2006).